HHS Public Access

Author manuscript

Cell Rep. Author manuscript; available in PMC 2024 February 05.

Published in final edited form as:

Cell Rep. 2023 October 31; 42(10): 113232. doi:10.1016/j.celrep.2023.113232.

Essential role of Mg^{2+} in mouse preimplantation embryo development revealed by TRPM7 chanzyme-deficient gametes

Neha Gupta[1,7], **Cristina Soriano-Úbeda**[1,2,7], **Paula Stein**[3], **Virginia Savy**[3], **Brian N. Papas**[4], **Goli Ardestani**[1,5], **Ingrid Carvacho**[6], **Dominique Alfandari**[1], **Carmen J. Williams**[3], **Rafael A. Fissore**[1,8,*]

[1]Department of Veterinary and Animal Sciences, University of Massachusetts, Amherst, MA 01003, USA

[2]Department of Veterinary Medicine, Surgery, and Anatomy, Veterinary School, University of León, León, Spain

[3]Reproductive & Developmental Biology Laboratory, National Institute of Environmental Health Sciences, National Institutes of Health, Research Triangle Park, NC, USA

[4]Integrative Bioinformatics Support Group, Biostatistics and Computational Biology Branch, National Institute of Environmental Health Sciences, National Institutes of Health, Research Triangle Park, NC, USA

[5]Clinical Research Embryologist, Boston IVF, Waltham, MA, USA

[6]Faculty of Medicine, Universidad Católica del Maule, Talca, Chile

[7]These authors contributed equally

[8]Lead contact

SUMMARY

TRPM7 (transient receptor potential cation channel subfamily M member 7) is a chanzyme with channel and kinase domains essential for embryo development. Using gamete-specific *Trpm7*-null lines, we report that TRPM7-mediated Mg^{2+} influx is indispensable for reaching the blastocyst stage. TRPM7 is expressed dynamically from gametes to blastocysts; displays stage-specific localization on the plasma membrane, cytoplasm, and nucleus; and undergoes cleavage that produces C-terminal kinase fragments. TRPM7 underpins Mg^{2+} homeostasis, and excess Mg^{2+} but not Zn^{2+} or Ca^{2+} overcomes the arrest of *Trpm7*-null embryos; expressing *Trpm7* mRNA

*Correspondence: rfissore@umass.edu.

AUTHOR CONTRIBUTIONS

N.G., C.S.Ú., and G.A. conducted and designed the experiments; N.G., C.S.Ú., P.S., V.S., B.N.P., and C.J.W. analyzed data and prepared the figures; D.A. provided technical assistance in the generation of monoclonal antibodies; N.G., C.S.Ú., and R.A.F. wrote the original draft of the manuscript; N.G., C.S.Ú., P.S., V.S., B.N.P., C.J.W., D.A., I.C., and R.A.F. edited the manuscript; R.A.F. supervised the research.

SUPPLEMENTAL INFORMATION

Supplemental information can be found online at https://doi.org/10.1016/j.celrep.2023.113232.

DECLARATION OF INTERESTS

The authors declare no competing interests.

restores development, but mutant versions fail or are partially rescued. Transcriptomic analyses of *Trpm7*-null embryos reveal an abundance of oxidative stress-pathway genes, confirmed by mitochondrial dysfunction, and a reduction in transcription factor networks essential for proliferation; Mg^{2+} supplementation corrects these defects. Hence, TRPM7 underpins Mg^{2+} homeostasis in preimplantation embryos, prevents oxidative stress, and promotes gene expression patterns necessary for developmental progression and cell-lineage specification.

Graphical Abstract

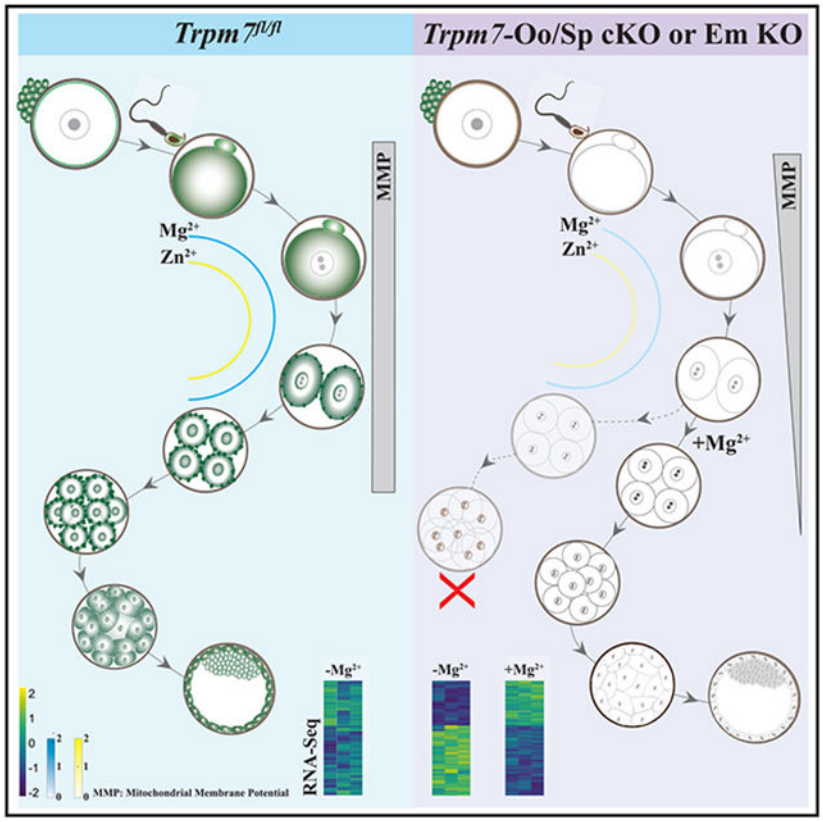

In brief

Gupta et al. identify the critical role of TRPM7 in embryos before the blastocyst stage. They show that the chanzyme is essential for Mg^{2+} homeostasis, and its kinase and channel domains cooperate to support development. In its absence, embryos exhibit oxidative stress, fail to proliferate, and undergo apoptosis and arrest.

INTRODUCTION

Divalent cations play essential functions in fertilization and early embryo development, including events associated with egg activation, implantation, and gastrulation.[1-4] The role of calcium (Ca^{2+}) in egg activation is universal, but the pattern of Ca^{2+} release changes across species. In mammals, the signal consists of repeated, brief rises in intracellular concentration lasting for several hours, which are known as Ca^{2+} oscillations.[3,5,6] The

realization that zinc (Zn^{2+}) contributes to fertilization is more recent, and the full scope of its effects remains incomplete.[7,8] Zn^{2+} undergoes exocytosis during fertilization, generating the Zn^{2+} sparks, and participates in the molecular control of meiosis exit post-fertilization and the polyspermy block.[9-11] Last, the precise role of magnesium (Mg^{2+}) in early development is unknown, despite the content of extracellular Mg^{2+} influencing the periodicity of Ca^{2+} oscillations and affecting embryo development.[12,13] Thus, divalent cations play essential roles in the initiation and progression of embryo development.

Gametes and embryos take up divalent cations from their environment using multiple specific and non-specific plasma membrane (PM) channels and transporters that remain incompletely characterized. Mammalian eggs and embryos express a complete Ca^{2+} tool kit,[3,14] but the molecules mediating Ca^{2+} influx have been investigated only in mouse eggs and early embryos.[15] Mouse eggs functionally express three Ca^{2+}-permeable channels: $Ca_V3.2$, a T-type voltage-gated channel (*Canah1h*),[16,17] and two transient receptor potential (TRP) family members, vanilloid-3[18] and melastatin-7 (TRPV3 and TRPM7, respectively).[15,19] Eggs null for any of these channels (conditional knockout [cKO] for *Trpm7*) mount somewhat altered Ca^{2+} responses after fertilization, and if paired with wild-type (WT) males, KO females display varying degrees of subfertility. *Trpv3*- or *Cacna1h*-null females are subfertile, even after homozygous mating or combined deletion,[20] contrasting with the early development arrest caused by the homozygous deletion of *Trpm7*.[21] A host of members of the solute carrier family 39 (*Slc39a1-14* or *Zip1-14*) and family 30 (*Slc30a1-10* or *ZnT1-10*) combine in a cell-specific manner to control the intracellular levels of Zn^{2+}.[22,23] However, their assortment and role in early development are untested. Oocytes highly express *Zip6* and *Zip10*[24] and embryos *Zip4*,[25] but thus far, only homozygous deletion of *Zip4* causes embryonic death by mid-gestation (for review, see Dufner-Beattie et al. and Hara et al.[25,26]). Several molecular transporters and buffering systems regulate the concentrations of free basal Mg^{2+} (approximately millimolar) in somatic cells.[27] However, hitherto, only genetic deletion of TRPM6 and TRPM7, which also conduct Mg^{2+}, impairs fertility and causes early embryonic death.[21,28-30] TRPM7 is notable among all the mentioned channels because of its widespread expression and permeability to Zn^{2+}, Mg^{2+}, and, to a lesser extent, Ca^{2+}.[31-33] It is unknown whether the absence of TRPM7 affects the transport of a combination of these cations in gametes and zygotes.

TRPM7 is a unique bifunctional molecule that, in addition to the channel domain, is outfitted on its intracellular C-terminal end with an active α-type serine-threonine kinase.[34] It is a cationic, non-selective channel with a permeability sequence favoring divalent cations that physiologically supports small inward currents.[31,32] TRPM7 forms active homomeric complexes and undergoes cleavage in a cell-type-specific manner that releases a C-terminal kinase (C-kinase) capable of nuclear translocation and histone phosphorylation.[35] Whether this occurs in gametes and embryos is unknown. The function of TRPM7 is essential for embryogenesis. TRPM7 ablation causes developmental arrest before embryonic day 7 (ED 7),[21,29] and a recent investigation found earlier demise of KO embryos, by ED 5, and failure of trophectoderm differentiation and implantation.[30] Neither study pinpointed the underlying molecular mechanism(s). Remarkably, the *Trpm7*-null embryos used in those studies resulted from heterozygous pairings, raising the possibility that, due to the oocytes' ability to synthesize and store mRNA and protein from the WT allele,[36] they may

retain levels of maternal TRPM7 post-fertilization, delaying KO embryos from acquiring null status. In support of this view, the pharmacological inhibitor of TRPM7, NS8593, caused embryonic arrest during cleavage stages,[15] suggesting that TRPM7 is essential at earlier stages of development than reported thus far by genetic studies. However, the expression, distribution, and function of TRPM7 in mammalian gametes and early embryos are unknown.

In this study, we examined the expression and role of TRPM7 in mouse gametes and preimplantation embryos. In oocytes, eggs, sperm, and cleaving embryos, TRPM7 expression is distinct and dynamic, and null gametes and embryos failed to accumulate TRPM7, with *Trpm7*-null zygotes failing to advance to the blastocyst stage. The absence of TRPM7 lowered Zn^{2+} and Mg^{2+} basal levels in eggs and embryos, but not that of Ca^{2+}, and did not prevent the initiation of Ca^{2+} oscillations. We further show that extracellular Mg^{2+} supplementation overcame the embryo development arrest and reversed the abnormal transcriptome of *Trpm7*-null embryos dominated by the expression of oxidative stress genes, dysfunctional mitochondria, and the downregulation of transcription factor networks involved in cell proliferation. *Trpm7* mRNA expression also rescued development in null zygotes, but a pore-deficient version did not, and a “kinase-dead” mutant did but only partially. Our results demonstrate the essential role of Mg^{2+} and TRPM7 in mammalian preimplantation development.

RESULTS

Conditional deletion prevents TRPM7 expression in gametes

Despite the essential role of TRPM7 in development, the stage of embryonic arrest and the molecular mechanism(s) underpinning it remain unresolved.[21,29,30] To address this question, we generated zygotes devoid of TRPM7. To this end, we produced a male-specific *Trpm7* cKO model using the *Hspa2*-Cre transgene, which is expressed in spermatocytes.[37] We employed a previously used *loxP* strain, *Trpm7*$^{fl/fl}$,[12,38] and crossed it with *Hspa2-Cre* or *Gdf9*-Cre lines to produce sperm- (*Trpm7*-Sp cKO) or oocyte-specific (*Trpm7*-Oo cKO) lines, respectively.[12] The deletion of *Trpm7* was confirmed by real-time PCR, as previously reported in eggs[12] and as shown here for sperm (Figure S1A).

We also confirmed the lack of protein expression in *Trpm7*-null gametes and investigated the currently unknown expression and distribution of TRPM7 in gametes and embryos. We produced a monoclonal antibody to accomplish this because available antibodies had low affinity and recognized TRPM6 and TRPM7.[39] We raised it against a fusion protein corresponding to a portion of the intracellular, C-terminal domain of mTRPM7. Western blot (WB) showed that germinal vesicle (GV) oocytes displayed strong reactivity at ~210 kDa (Figure 1A, left lane, red arrow), consistent with the molecular weight (MW) of TRPM7 in cells[34] and with our results in oocytes.[39] Metaphase II (MII) eggs also showed reactivity at this approximate MW but with less intensity and shifted upward, possibly reflecting phosphorylation (Figure 1A, middle lane), a common modification of TRPM7.[40] The ~210 kDa signal was absent in *Trpm7*-Oo cKO GV oocytes (Figure 1A, right lane). GV oocytes also showed lower MW bands, consistent with earlier findings that TRPM7 undergoes cell-specific cleavage upstream of the kinase domain, generating C-terminal products.[35,41]

We observed three prominent bands of ~115, 70, and 45 kDa (Figure 1A, arrowheads), which were not detected or were of lower intensity in MII eggs and were absent in null oocytes. Brain, testes, and sperm also expressed TRPM7 and displayed an ~210 kDa band corresponding to full-length TRPM7 (Figure 1B, middle lanes). The testes of *Trpm7*-Sp cKO males showed less TRPM7 reactivity, congruent with TRPM7 expression in testicular cells other than sperm (Figure 1B, third lane), but sperm lacked reactivity altogether (Figure 1B, right lane). Further, testes and sperm also displayed C-terminal products with distinct MWs (Figure 1D, arrowheads).

We next examined the location of TRPM7 in *Trpm7*$^{fl/fl}$ gametes using immunofluorescence (IF). At threshold intensities, TRPM7 adopts a uniform PM localization in GV oocytes (Figure 1C, upper row, center and right; arrow), while MII eggs display an un-even PM distribution punctuated by a few clusters and increased cortical and cytoplasmic reactivity (Figure 1C, lower row, center and right; arrows). In addition to the change in distribution, the signal in MII eggs was less intense, as evidenced by the negligible fluorescence when these cells were exposed to the GV's threshold intensity (Figures S1B and S1C, top), and vice versa, the additional appearance of a cytosolic signal in GVs when exposed to the threshold intensity of MII eggs (Figures S1B and S1C, bottom). These results are consistent with our electrophysiological characterization of TRPM7 function in these cells.[15]

TRPM7's cytosolic reactivity in somatic cells does not colocalize with markers of known cellular compartments.[42] To determine whether the cytosolic distribution of TRPM7 in eggs corresponded to the location of the ER or internal lipid vesicles that are present throughout the ooplasm, we expressed the D1-ER construct[43] or stained eggs with BODIPY (500/510), respectively, and examined their fluorescent signals. We did not observe a significant overlap between TRPM7 and these structures, indicating that they are not TRPM7's hosting organelles in eggs, whose determination will require additional studies (Figure S1D). We also tested our antibody's specificity by examining whether *Trpm7*-Oo cKO oocytes and eggs lacked TRPM7 reactivity (Figure 1D), which was indeed the case. Granulosa cells from *Trpm7*-Oo cKO cumulus displayed staining (Figure 1D; arrowhead), as did granulosa cells of *Trpm7*$^{fl/fl}$ females (Figure 1C; arrowhead), consistent with the presence of *Trpm7* transcripts in these cells.[44] Lastly, sperm showed diffuse reactivity in the head but not in the tail; this reactivity was absent in *Trpm7*-Sp cKO sperm (Figure 1E). Our data confirm that the conditional deletion approach of *Trpm7* effectively depletes the protein from gametes and shows that gametes distinctively express TRPM7.

TRPM7 is indispensable for preimplantation embryo development and fertility

We first examined the fertility of the gamete-specific *Trpm7* cKO lines by pairing them with the corresponding male/female *Trpm7*$^{fl/fl}$ counterparts that express normal levels of TRPM7 and recorded their fecundity parameters. *Trpm7*$^{fl/fl}$ homozygous crosses produced a mean litter size of 6.5 ± 1.8 pups, comparable with pairs using *Trpm7*-Sp cKO sires, consistent with sperm analyses demonstrating that the *Hspa2-Cre* transgene had negligible effects on sperm production or function (Tables S1 and S2; $p > 0.05$). In contrast, consistent with previous findings,[12] mating pairs using *Trpm7*-Oo cKO dams produced smaller litters (Figure 2A, left; ****$p < 0.0001$). In addition, both *Trpm7*-gamete-specific lines generated

less than half of the total number of pups and parturitions compared with *Trpm7*$^{fl/fl}$ pairs, reinforcing the requirement of TRPM7 for embryo development (Figure 2A, center and right, respectively; $p < 0.05$). Expectedly, crossing *Trpm7*-Oo females and *Trpm7*-Sp cKO males failed to produce offspring (Figure 2A, left; $p < 0.05$).

To discover the timing of the arrest of *Trpm7*-embryo (Em) KOs during development, we monitored every 24 h the progression of zygotes to the blastocyst (BL) stage. Zygotes produced after mating or *in vitro* fertilization (IVF) were cultured *in vitro* for the study (Figures 2B-2D). Regardless of origin, *Trpm7*-Em KO zygotes were unsuccessful in becoming BLs, with only a fraction of *in vivo*-produced zygotes developing into BLs (Figures 2B-2D; $p < 0.05$). We parsed these data to establish if the developmental block displayed a stage preference. Nearly all zygotes, defined as those with identifiable pronuclei (PNs) at 8 h post-fertilization, cleaved to the two-cell (2C) stage, but successive cleavages showed attrition that was most evident between the 2C and the 4C and between the 4C and the 8C stage transitions, with most of the few morulae failing to advance to BLs (Figures 2B-2D; $p < 0.05$). Last, the few embryos that became BLs had abnormally low cell numbers (Figure 2C; $p < 0.05$), unlike *Trpm7*$^{fl/fl}$ zygotes, which developed to BLs at high rates (Figures 2B-2D) and displayed the expected number of cells (Figure 2C; $p < 0.05$). We next examined whether higher rates of cellular apoptosis could at least partly explain the lower cell numbers in null BLs. This was the case, as whereas the majority of *Trpm7*-Em KO BLs had TUNEL-positive cells, this was not the case for control BLs (Figures 2E and 2F), suggesting that cell death may compromise the development of *Trpm7*-Em KO BLs.

To confirm the preimplantation *in vitro* results, we collected embryos from females at different times post-mating. We flushed oviducts at 36 and 60 h post-ovulation, ~1.5 and 2.5 dpc, to collect 2C and 8C embryos, respectively.[45] Our *in vivo* results confirmed the *in vitro* data, as, in addition to retrieving approximately the same number of embryos per female, *Trpm7*$^{fl/fl}$ and *Trpm7* cKO pairs produced similar numbers of 2C embryos, but *Trpm7* cKO pairs had fewer 8Cs along with higher numbers of 4Cs (Figures S2A and S2B), demonstrating developmental delay. Additional *in vitro* culture of the *in vivo*-generated 2C and 8C embryos failed to produce BLs (Figure S2C). Together, these results indicate that TRPM7 plays an essential role in mammalian development starting at the early cleavage stages and is indispensable beyond the 8C stage.

TRPM7 displays stage-specific expression and distribution during preimplantation embryo development

To elucidate the basis of the essential role of TRPM7 in embryos, we first investigated the expression and cellular localization of the chanzyme in preimplantation embryos. We confirmed that GV oocytes express the ~210 kDa band corresponding to the full-length TRPM7 (M7-FL), whose intensity declined in MII eggs. In zygotes (PN), the 210 kDa band remained low, as displayed in the blot where all embryo stages were handled concurrently (Figure 3A, first three columns from the left; red arrow). The intensity of the M7-FL band remained low in 2C embryos but increased in 4C and 8C stage embryos, consistent with the onset of the zygotic transcription at the 2C stage (Figures 3A, three center columns, and 3B; $p < 0.05$). Morula stage embryos experienced a marked decline in the reactivity

of the M7-FL band, which rebounded in BLs (Figure 3A, two rightmost columns; red arrow; $p < 0.05$). The C-terminal products of TRPM7 (M7-CTs) also showed pronounced changes in expression throughout the preimplantation stages (Figures 3A, red arrow-heads, and 3B), suggesting TRPM7 undergoes targeted cleavages. Given their estimated sizes, these fragments likely contain the kinase domain of the chanzyme.

We next examined the cellular localization of TRPM7 on *in vivo*-fertilized zygotes cultured *in vitro* to the specified stage. We also located other cellular landmarks by DNA staining, the nucleus, and by actin staining, the cortical area near the PM. The rightmost column displays the integrated profiles of these signals (Figure 3C). Like in MII eggs, the presence of TRPM7 in zygotes was predominantly cytosolic (Figure 3C, top row). In 2C embryos, despite retaining cytoplasmic staining, the distribution of TRPM7 noticeably changed. In the PM/cortex, TRPM7 appeared in regularly spaced cluster-like accumulations (Figure 3C, second row; yellow circle in the zoomed-in image), whereas a nascent aggregation became evident in the nucleus (Figure 3C, second row; yellow arrowhead in the zoomed-in image). TRPM7 reactivity of any kind was absent in 2C and 4C *Trpm7*-Em KO embryos, confirming the specificity of our antibody (Figure S3A). Four-cell stage embryos showed larger PM/cortical clusters accompanied by increased nuclear localization and decreased cytoplasmic reactivity (Figures 3C, third row, and 3D; $p < 0.05$). As in the previous stage, 8C embryos displayed larger PM/cortical clusters and nuclear distribution (Figure 3C, fourth row). The intensity of TRPM7 reactivity seemed lowest at the morula stage, without distinct PM clusters, and regained diffuse cytoplasmic staining while maintaining nuclear localization (Figure 3C, fifth row). In BLs, the distribution of TRPM7 also seemed to be nuclear and cytoplasmic, with the outer cells part of the trophoblast showing an almost homogeneous distribution of TRPM7 between the nucleus and the cytoplasm (Figure 3C, sixth row), while the internal cells that likely correspond to the inner cell mass (ICM) appear more intensively reactive on the cytoplasm/cortex (Figure S3B). Collectively, the dynamic expression and localization of TRPM7 throughout preimplantation development with the concurrence of PM and nuclear localizations in specific stages are consistent with TRPM7's vital role in preimplantation embryo development and differential contributions of its channel and kinase domains.

Loss of TRPM7 impairs divalent cation homeostasis in eggs

The widespread expression and distinct distribution of TRPM7 in gametes and embryos and its preferred permeability for divalent cations[32] predict a pivotal role in their homeostasis in early development. We used cation-specific fluorescent dyes first to estimate their intracellular concentrations in MII eggs. Ca^{2+} and strontium (Sr^{2+}) were unchanged in *Trpm7*$^{fl/fl}$ control eggs and in *Trpm7*-Oo cKO eggs (Figure 4A, left two plots; $p > 0.05$), consistent with the ability of *Trpm7*-Em KO zygotes to initiate Ca^{2+} oscillations in response to fertilization with normal individual Ca^{2+} rise parameters (Figures S4A-S4C and data not shown); the reduced frequency is consistent with a previous report showing lower periodicity responses when using eggs from this null line[12] (Figures S4A-S4C; $p < 0.05$). Remarkably, Zn^{2+} and Mg^{2+} were significantly lower in *Trpm7*-Oo cKO eggs (Figure 4A; $p < 0.05$). These results extend previous electrophysiological demonstrations that TRPM7 is

functionally active in oocytes and eggs[12,15] and suggest pivotal contributions to Zn^{2+} and Mg^{2+} homeostasis in these cells.

The unchanged levels of Ca^{2+} in *Trpm7*-Oo cKO eggs contrast with results by others that showed that *Trpm7*-null 2C embryos displayed lower basal Ca^{2+} in addition to reduced Mg^{2+} concentrations.[30] To ascertain whether the levels of Ca^{2+} progressively changed during embryo progression and whether other divalent cations remained low, we evaluated their intracellular levels in *Trpm7*-Em KO 4C embryos. We selected this stage because blastomeres are amenable to individual monitoring, TRPM7 adopts distinct positioning, and the development of many *Trpm7*-null embryos stalls at this stage. The Ca^{2+} levels were undisturbed in 4C *Trpm7*-Em KOs (Figure 4B, left), but Mg^{2+} and Zn^{2+} concentrations remained low, especially the former (Figure 4B, right and center, respectively; $p < 0.05$). These results suggest that TRPM7 is mainly responsible for Mg^{2+} homeostasis in eggs and preimplantation embryos. In this vein, we evaluated whether Mg^{2+} concentrations spontaneously changed in $Trpm7^{fl/fl}$ embryos during the first divisions. We found that Mg^{2+} levels remained steady throughout the early cellular divisions despite the changes in cellular distribution that TRPM7 experiences in these embryos (Figure S5).

Mg^{2+} but not Zn^{2+} supplementation rescues the arrest of *Trpm7*-Em KO zygotes

Given that the absence of TRPM7 expression significantly lowered the intracellular concentrations of Mg^{2+} and Zn^{2+} in eggs and embryos, we examined whether supplementing these cations could overcome the developmental arrest that *Trpm7*-Em KO embryos experience. *In vivo*-produced zygotes were cultured from the 2C stage until the BL stage in medium with 10 mM $MgCl_2$, 10 μM $ZnCl_2$, or a combination of these ions (Figure 5A). Supplementing external Mg^{2+} restored BL rates but increasing Zn^{2+} did not (Figures 5B-5D; $p < 0.05$), and together they rescued development, but at lower rates than Mg^{2+} alone (Figures 5D and 5E; $p < 0.05$), possibly reflecting competition among these cations for influx or, alternatively, Zn^{2+} inhibition of the putative Mg^{2+} influx molecules. Mg^{2+} supplementation also increased BL cell numbers without reaching the numbers of the supplemented controls (Figure 5D; $p < 0.01$). These results suggest that TRPM7 is essential for Mg^{2+} homeostasis in preimplantation embryos.

We next investigated when the demands for Mg^{2+} increased in preimplantation embryos. We delayed supplementation until the 4C or 8C stage (Figure S6A) and monitored *in vitro* development as above. Adding Mg^{2+} at the 4C stage rescued BL development rates, but not cell numbers (Figures S6B and S6C; $p > 0.05$, $p < 0.0001$, respectively), and at the 8C stage did not recover either parameter but still supported development to the BL stage (Figures S6D and S6E; $p < 0.01$, $p < 0.0001$, respectively). These results suggest that the demand for Mg^{2+} increases from the 2C stage onward, which is when expression of *Trpm7* increases in preimplantation embryos to remain at high levels thereafter[46,47] (KOMP-sponsored website: https://blogs.umass.edu/jmager/early-gene-expression/); it also coincides with the activation of transcription and the major zygotic gene activation (ZGA) milestone in 2C mouse embryos.

We performed a BL outgrowth assay to determine whether the Mg^{2+} requirement extended past the BL stage. $Trpm7^{fl/fl}$ and *Trpm7*-Em KO zygotes were cultured in 10 mM Mg^{2+}

until the BL stage. Then, BLs were transferred to conditions with different extracellular Mg^{2+} concentrations of 0.8, 1.8, and 10 mM, which are the concentrations in DMEM, in the uterus, and required for rescue, respectively. While *Trpm7*$^{fl/fl}$ BLs hatched and expanded at all Mg^{2+} concentrations, almost none of the *Trpm7*-Em KO BLs hatched in 0.8 mM Mg^{2+}, but most did at 1.8 mM Mg^{2+}, although without expansion, and 10 mM Mg^{2+} was necessary for *Trpm7*-Em KO BLs to behave as controls (Figures 5F and 5G; $p < 0.05$). These results demonstrate the continuous Mg^{2+} and TRPM7 requirement during preimplantation and initial implantation stages.

Trpm7^{wt} mRNA, but not mutant versions, fully rescues the development of *Trpm7*-Em KO zygotes without Mg^{2+} supplementation

To demonstrate that TRPM7 underpinned the arrest of *Trpm7*-Em KO zygotes, we injected *Trpm7*^{wt}-*Venus* mRNA into *in vivo*-fertilized *Trpm7*-Em KO zygotes (Figure 6A) to assess the ability to promote development to the BL stage without Mg^{2+} supplementation. We confirmed mRNA translation by live fluorescence and VENUS visualization (Figure S7). The heterologous protein successfully restored cleavage rates and BL cell numbers to the levels of control embryos (Figures 6A-6C; $p > 0.05$). TRPM7^{wt}-VENUS achieved a distribution similar to that of the endogenous protein in 2C and 4C embryos, although with minor differences such as accumulation on the nuclear membrane, lesser concentration in the nucleus, and PM localization but with less conspicuous clusters, possibly due to the VENUS tag on the C-terminal end of the molecule (Figure S7).

To examine in detail whether only the channel portion of the TRPM7 was required for embryo development, we mutated it to generate a channel pore mutant, *Trpm7*^{P1040R}, a truncated molecule without the kinase domain *Trpm7*^{1570Stop}, or a kinase-dead version, *Trpm7*^{K1646R}.[41,48-50] mRNAs for all mutants were injected as above, and embryo development followed; the injection of *Trpm7*^{wt} mRNA served as the positive control. The *Trpm7*^{P1040R} pore mutant and the kinase-less chanzyme failed to rescue embryo development, and the channel pore mutant also prevented the development of WT embryos, acting in a dominant-negative-like manner (Figures 6D and 6E), confirming findings by others of inactivation of native channels by expression of the pore mutant form.[48] Expression of the *Trpm7*^{K1646R} mRNA rescued embryo development but not to the same extent as *Trpm7*^{wt} mRNA: ~40% less (Figure 6F). Collectively, these results validate the essential role of TRPM7 in embryo development and Mg^{2+} homeostasis and suggest that both domains of the chanzyme contribute to promoting the optimal function of the chanzyme.

Trpm7-Em KO embryos experience oxidative stress and have abnormal transcriptome profiles rescued by Mg^{2+} supplementation

We performed transcriptome profiling of MII eggs and embryos through the morula stage to identify the molecules and pathways undermining the development of *Trpm7*-Em KO zygotes. There were few differentially expressed genes (DEGs) in MII eggs (153) and 2C embryos (17), but these numbers progressively increased from the 4C to the morula stage (Figure 7A; Table S3). We applied Ingenuity Pathway Analysis (IPA) to evaluate canonical pathways and upstream regulators that could explain the developmental differences between

control and *Trpm7*-Em KO embryos. At the 4C stage, too few DEGs were available to carry out a pathway analysis, but IGF1 signaling was among the activated upstream regulators (Figure 7B). Notably, 50% (6/12) of the DEGs driving the identification of IGF1 have roles in mitochondrial function, inflammation, or oxidative stress. In 8C embryos, almost all the significant canonical pathways identified showed an association with oxidative stress (Figure 7C; Table S4). This theme persisted in the morula stage, although canonical pathways involved in cell proliferation and embryo development were also identified here (Figure 7D; Table S4). We confirmed the transcriptomic changes by qPCR assessment of nine genes selected from the RNA sequencing (RNA-seq) datasets and involved in oxidative and ER stress, gene expression, and TRPM7 channel regulation (Figure S8A). In addition, to test for physiological evidence of oxidative stress, we examined the mitochondrial membrane potential (MMP). MMP was similar in MII eggs of both groups, but in *Trpm7*-Em KO embryos, starting at the 2C stage, the MMP progressively declined through 8C relative to stage-matched controls (Figures 7E and S8B). These results are consistent with oxidative stress underlying the continuous decline of embryo development in cleaving *Trpm7*-null embryos.

We next tested whether Mg^{2+} supplementation could rescue the abnormal transcriptome of *Trpm7*-Em KO embryos, as it did embryo development. Two-cell *Trpm7*-Em KO and control embryos were supplemented or not with 10 mM Mg^{2+} and collected 24 and 48 h later. After 24 h culture, RNA-seq revealed 295 DEGs comparing controls to *Trpm7*-Em KO embryos, but Mg^{2+} supplementation almost returned the transcriptome to normal in 24 h, because only 19 DEGs remained in the $+Mg^{2+}$ group (Figure 7G; Table S5). By 48 h, there were 830 DEGs comparing controls to *Trpm7*-Em KO embryos, but only 5 DEGs in the $+Mg^{2+}$ group. Indeed, unsupervised hierarchical clustering no longer sorted the Mg^{2+}-supplemented separately from the control embryos (Figure 7H). Consistent with these results, we show that Mg^{2+} supplementation rescued intracellular levels of Mg^{2+} (Figure S8C) and MMP values (Figures 7F and S8D). These results highlight the determinant role of TRPM7 during preimplantation embryo development in regulating Mg^{2+} homeostasis, which is vital for gene expression and developmental competence of early embryos. It also suggests that the Mg^{2+} imbalance is responsible for the oxidative stress undermining *Trpm7*-Em KO development.

DISCUSSION

Here, we showed that TRPM7-mediated Mg^{2+} influx is required for early embryo development because *Trpm7*-null zygotes displayed diminished Mg^{2+} levels and failed to progress to the BL stage. This arrest is significantly earlier than in previous reports that paired *Trpm7*-heterozygous mice. TRPM7 adopts distinct and dynamic localization in oocytes, eggs, and early embryos. Ablating it, in addition to affecting Mg^{2+}, reduced the intracellular levels of Zn^{2+} and caused widespread alteration of the transcriptome and oxidative stress. Mg^{2+} supplementation alone entirely rescued embryo development, as did *Trpm7*^{wt}-*Venus* mRNA expression. These results establish that aberrant Mg^{2+} homeostasis underlies the inability of *Trpm7*-Em KO embryos to complete development, providing a mechanistic understanding of the vital role of TRPM7 in preimplantation embryo development and defining the timing of the arrest. The coexistence of TRPM7

in distinct cellular compartments in specific embryo stages suggests varied contributions of the chanzyme to underpin embryo development in mammals.

The role of TRPM7 in divalent cation homeostasis is well documented,[31,34] but the ions regulated vary widely among cell types and systems. Earlier studies showed that TRPM7 participated in Mg^{2+} homeostasis, because B lymphocytes and other cell types without *Trpm7* failed to proliferate, a defect rescued by Mg^{2+} supplementation.[28,34,51] However, Mg^{2+} did not rescue all *Trpm7*-mutant cell lines, some of which showed altered levels of Zn^{2+} or Ca^{2+} and not Mg^{2+}.[35,42,52-54] Here, we found that TRPM7 is the essential Mg^{2+}-conducting channel in preimplantation mouse embryos beyond the 4C stage, as without it, embryonic arrest and developmental failure ensue. The mechanistic insights into the role of TRPM7 gleaned from our studies may extend to the embryo development of other vertebrates.[55,56]

It is unknown why TRPM7 is essential for some cells and tissues and not for others. Gametes and zygotes are endowed with robust and alternate systems that ensure the steady supply of Ca^{2+} and Zn^{2+} even in the event of loss or malfunction of a channel(s) because of their indispensable roles in meiosis, fertilization, and early development.[12,17,18] The expression of Mg^{2+} transporters in mammalian oocytes, eggs, and embryos remains unexamined, despite transcriptomic information revealing that several of the common Mg^{2+} transporters and antiporters[57] are detectable in mouse zygotes and embryos, such as *Trpm6* and two members of the cyclin and CBS domain divalent metal cation transport mediator family (CNNM), *Cnnm1* and *Cnnm4*.[47] Based on our results in oocytes and early embryos, these molecules are unable to compensate for the absence of TRPM7, at least at the physiological levels of external Mg^{2+} and during the first approximately two-thirds of the pregnancy, because deletion of *Trpm7* after E14 does not appear to affect litter size.[21] Given the role of Zn^{2+} in gene expression and the lower levels of Zn^{2+} in *Trpm7*-Em KO embryos, we cannot rule out a role in diminishing the developmental competence of these embryos despite its supplementation being unable to rescue development.

The low levels of Mg^{2+} in *Trpm7*-null eggs remained so in 4C embryos and through the BL stage, congruent with a previous report showing lower Mg^{2+} levels in *Trpm7*-null 2C embryos from heterozygous crosses.[30] It is unclear when TRPM7 becomes essential for Mg^{2+} homeostasis during oogenesis and folliculogenesis. *Trpm7*-Oo cKO females produce the expected number of functional oocytes and eggs after hormonal stimulation, implying that Mg^{2+} demands are lower during this process or met by other channels or transporters until ovulation. Granulosa cells, the nurse cells of the ovary, are in intimate contact with oocytes throughout folliculogenesis, allowing the exchange of metabolites and cell products during this process.[58] Analyses of transcriptomic profiles reveal the expression of *Trpm7* in granulosa cells (UniProtKB: Q96QT4 and Q923J1),[59] which we confirmed by IF studies. It is noteworthy that RNA-seq and microarray studies suggest an association between the expression of *Trpm7* in cumulus cells and pregnancy rates in assisted reproductive technologies (ART) patients.[60] Therefore, the cumulus-oocyte complex organization may support folliculogenesis in *Trpm7*-Oo cKO females. We also show that spermatozoa express TRPM7 but did not examine the functional expression and possible role(s) in these cells. The localization in the sperm head and absence in the tail suggest TRPM7 is not involved

in the regulation of motility, and its role in cation homeostasis,[41] if any, may occur earlier during spermatogenesis.

TRPM7 expression is widespread and detected in almost every tissue and cell type.[31,61,62] Its subcellular localization runs the gamut of PM, cytoplasm, and nucleus.[35,42,63] The expression and localization of TRPM7 in gametes and embryos were unknown until this study. We discovered that it is expressed with remarkable precision and distinct localization throughout the preimplantation stages. Further, we observed a decline in the reactivity of the full-length protein from the GV stage to the end of maturation at the MII stage, remaining low until the 4C stage; this is consistent with our IF results. We are uncertain whether the reduced reactivity is due to TRPM7's degradation or post-translational modifications that interfere with epitope recognition. The section of TRPM7 used to raise the antibody is the target of post-translational changes,[40] which may obstruct antibody recognition. Further, the C-terminal products of TRPM7 resulting from its proteolytic processing detected in somatic cells[35,41] are also recognized in GVs and embryos and displayed stage-specific differential expression that follows that of the full-length protein. Future studies should examine the enzymes and proteases that modify the chanzyme and their functional consequences.

In MII eggs and zygotes, TRPM7 shows predominant cytoplasmic accumulation. TRPM7 also displays cytoplasmic localization in somatic cells and associates with glutathione-rich internal vesicles.[42] It is unknown whether this happens in eggs and zygotes and whether the cytoplasmic expression represents the full-length TRPM7 or its C-terminal fragments. From the 2C to the 8C stage, TRPM7 in the PM/cortex becomes organized in prominent clusters, achieving a "pearls-on-a-string" appearance. This organization may have functional consequences and an impact on TRPM7's whole-cell currents, which rebound in 2C following inactivation in MII eggs[15] despite TRPM7's apparent expression remaining unchanged. Future studies will investigate whether clustering and size have an impact on the permeability and ion selectivity of TRPM7 and elucidate the other components of this likely complex. It will be interesting to discover whether TRPM7's expression and function contribute to the *de novo* polarization that unfolds in 8C embryos.[64,65] This step requires cortical recruitment of actomyosin[65] and depends on myosin IIA phosphorylation, a substrate of TRPM7.[63] Finally, the nuclear accumulation of TRPM7 is first evident at the 2C stage, increases in 4C and 8C blastomeres, and is retained in morulae and BL blastomeres. The role of TRPM7 in the nucleus of blastomeres is unknown, but in somatic cells, the C-terminal kinase products bind chromatin-remodeling complexes and phosphorylate histone H3 serine residues.[35] The zygotic genome becomes activated following fertilization, and remodeling of the parental genomes ensures normal development. DNA and protein modifications, DNA accessibility, and transcription factors instruct this closely regulated transition.[66-68] Therefore, the nuclear localization of TRPM7 in preimplantation embryos may influence the remodeling of the genome and gene expression during embryogenesis. The reduced expression of transcription factors and associated regulatory networks in *Trpm7*-Em KO embryos support this possibility.

The demonstration that only Mg^{2+} supplementation restored *Trpm7*-Em KO's developmental rates and BL composition confirmed TRPM7's essential role in Mg^{2+} homeostasis. Mg^{2+} demands increase sharply between the late zygote and the 4C stage

because, after this time, supplementation does not recover embryo development or BL cell numbers. Mg^{2+} supports the functions of hundreds of enzymes and is synonymous with cellular growth and metabolism.[50,69] Consequently, these early embryos, which require new gene expression and activation of the embryonic genome, and where timely cell division and differentiation are necessary for forming a new organism, are susceptible to Mg^{2+} deficiency, which promptly interrupts developmental progression. Cancer cells display similar demands and dependency for Mg^{2+} [70] and routinely show enriched expression of molecules that favor its transport.[71,72] Mg^{2+} deficiency is a common cause of oxidative stress and inflammation-induced oxidative stress that underlies the development of many cancers.[70,73] Congruent with this, IPA of DEGs in *Trpm7*-Em KO 4C and 8C embryos showed an overrepresentation of canonical oxidative stress pathways. These changes translated into metabolic consequences indicative of oxidative stress and compromised mitochondrial function, confirmed by decreasing JC-1 fluorescence ratios in *Trpm7*-Em KO embryos. Remarkably, transcriptomic analyses of liver samples from *Trpm6* KO mice and intestinal samples from organ-specific *Trpm7* KO 5-day-old pups also displayed gene expression changes consistent with oxidative stress, suggesting this might be the prototypical gene response to hypomagnesemia.[28,54] Mg^{2+} supplementation at the 2C stage also reversed the transcriptomic changes of *Trpm7*-Em KO embryos, indicating that aberrant Mg^{2+} homeostasis underlies most of the transcriptomic, metabolic, and developmental changes that prevent these embryos' progress. These results imply that the channel, not the kinase activity of TRPM7, is essential for embryo development. Nevertheless, we cannot rule out altered gene expression or epigenome in *Trpm7*-Em KO embryos or offspring, mainly because Mg^{2+} supplementation does not fully restore *Trpm7*-Em KO BL cell numbers. Furthermore, we show that, whereas injection of *Trpm7*^{wt}-*Venus* mRNA rescued the development of *Trpm7*-null embryos, expression of the *Trpm7*^{K1646R} kinase-dead mutant was far less successful, pointing to a possible contribution of the kinase domain to embryo development. Future studies will examine whether it accomplishes this by modifying the channel's function or influencing gene expression. Collectively, these results validate the essential role of TRPM7 in embryo development and Mg^{2+} homeostasis and suggest that all domains contribute to promoting the optimal function of the chanzyme.

In summary, TRPM7 is essential for Mg^{2+} homeostasis in preimplantation embryos. Our results add a third divalent cation, in addition to Ca^{2+} and Zn^{2+}, whose regulated availability is indispensable for the successful initiation of development. Its insufficiency causes oxidative stress and transcriptional aberrations. In addition to being expressed in both gametes and embryos, we show that TRPM7 adopts dynamic and stage-specific expression and localizations that enable its ionic and molecular functions. Elucidation of the partners and regulators that underpin its pervasive presence in preimplantation embryos will provide insights into factors that buttress cell proliferation, differentiation, and embryonic development.

Limitations of the study

There are several limitations to contemplate when considering our paper. We have not yet identified the target epitope of our monoclonal antibody. While it has made it possible to analyze the expression and distribution of TRPM7 in gametes and embryos, and the absence

of reactivity in null gametes and embryos confirms its specificity, it does not distinguish whether the lower TRPM7 signal in MII eggs and zygotes vs. GV oocytes and later embryo stages is due to degradation or phosphorylation; the portion of TRPM7 used to raise it contains multiple phosphorylation sites, which might compromise its binding affinity. We will use previously untested antibodies developed by colleagues to address this. Similarly, our available methods do not allow us to resolve whether TRPM7's cytosolic signal in MII eggs, zygotes, and BL stage consists of the FL-TRPM7 or its cleavage products and if, following cleavage of TRPM7, the channel portion stays on the PM or is internalized or degraded. On this same topic, we cannot determine the organelle(s) associated with TRPM7 in the cytosol, and more exhaustive studies with organelle markers will be required. Also, TRPM7 in eggs and embryos shows varied PM and cortical localizations. How they affect channel function across all the stages will demand optimization of the electrophysiological approaches and embryo manipulation, as blastomeres must be isolated to perform the recordings. Our results show that both domains of the chanzyme contribute to optimizing embryo development; the nuclear localization displayed by TRPM7 in certain embryo stages suggests tantalizing roles in chromatin organization and gene expression. However, additional studies are needed to precisely identify the significance of this function and the gene(s) affected. Last, the dominant-negative-like effects displayed by the expression of the *Trpm7*^{P1040R} mRNA that causes abrupt embryo developmental arrest raise questions regarding how it disrupts channel function and the role of Mg^{2+} homeostasis in early development.

STAR★METHODS

RESOURCE AVAILABILITY

Lead contact—Further information and requests for resources and reagents should be directed to and will be fulfilled by the lead contact, Rafael Fissore (rfissore@umass.edu).

Materials availability—All the plasmids and antibody generated during this study is available to share from the lead contact and will be sent to national repositories.

Data and code availability

- All data generated during this study are available to share from the lead contact.
- The sequencing data generated in this study have been deposited in the Gene Expression Omnibus database under accession code GSE241487 and are publicly available as of the date of publication.
- Any additional information required to reanalyze the data reported in this work is available from the lead contact upon request.

EXPERIMENTAL MODEL AND STUDY PARTICIPANT DETAILS

This study only used mouse models of the strains listed below. Females used to collect oocytes and, embryos were between 6 to 10 weeks old. When embryos were collected and mating was required, the age of males was between 8 to 10 weeks. The University of Massachusetts Institutional Animal Care and Use Committee (IACUC) approved all animal

experiments and protocols. Balbc, *Trpm7*$^{fl/fl}$, *Hspa2-Cre*, and *Gdf9-Cre* mice, generated from a mixed background of C57BL6/J and 129s4/SvJae, were gifts from Dr. Carmen Williams (NIEHS, USA) or purchased from The Jackson Laboratory (Jackson Labs, Bar Harbor, ME), and bred at our facility. *Trpm7*-floxed (*Trpm7*$^{fl/fl}$) mice were crossed with *Trpm7*$^{fl/fl}$-*Hspa2-Cre* and *Trpm7*$^{fl/fl}$-*Gdf9-Cre* breeders to produce sperm-specific (*Trpm7*-Sp conditional knockout (cKO)) and oocyte-specific (*Trpm7*-Oo cKO) *Trpm7* cKO mouse lines, respectively. Whole KO embryos (*Trpm7*-Em KO) were obtained by crossing gametes from the *Trpm7*-gamete specific KO lines and controls from mating *Trpm7*$^{fl/fl}$ breeders.

METHOD DETAILS

Mice, genotyping, and PCR analysis—Mice were genotyped using tissue from an ear clip collected and lysed using tail lysis buffer (50 mM Tris-HCl pH 8.8, 1 mM EDTA pH 8, 0.5% Tween 20, 0.3 mg/ml proteinase K). Genomic DNA was stored at −20°C and used later for PCR analysis. PCR products were used to determine genotypes following their separation on a 1.2% agarose gel following standard procedures, as previously performed in our laboratory[39].

***In vivo* fertility of *Trpm7*-modified genetic lines—**The fertility of gamete-specific and embryo-deleted Trpm7 lines was evaluated by mating six pairs per genetic line for six months and recording the outcomes of these pairings. The following parameters were considered, the number of total parturitions, total number of pups, and pups per litter. The following crosses were evaluated (male x female): *Trpm7*$^{fl/fl}$ x *Trpm7*$^{fl/fl}$, *Trpm7*-Sp KO x *Trpm7*$^{fl/fl}$, *Trpm7*$^{fl/fl}$ x *Trpm7*-Oo KO, and *Trpm7*-Sp KO x *Trpm7*-Oo KO.

RNA isolation and RT-PCR—Total RNA was extracted from the sperm of *Trpm7*$^{fl/fl}$ and *Trpm7*-Sp cKO males using the High Pure RNA isolation kit (Roche, Cambridge, MA) and following the manufacturer's instructions. 1x10^6 sperm were used to extract total RNA, 1μg of which was used for the additional procedures. For embryos, total RNA was extracted from 25 *Trpm7*$^{fl/fl}$ and *Trpm7*-Em KO 4C embryos. Reverse transcription was performed using an iScript cDNA synthesis kit (Bio-Rad, Hercules, CA). Real-time PCR was performed using the Power SYBR™ Green PCR Master Mix (Thermo Fisher, Agawam, MA). *Actb* was used as an internal control for normalization. The Mx3000 Real-Time PCR System (Agilent Technologies, Santa Clara, CA) was used to amplify the products of the reaction, and quantification of these RNA products' was performed by normalizing to *Actb* using the comparative C_T methodology, as described.[74]

Gametes, zygotes, and preimplantation embryo culture and collection—Gametes and zygotes were collected and processed as previously described.[20,39] Briefly, 6- to 10-week-old females were intraperitoneally (IP) injected with pregnant mare's serum gonadotropin (PMSG, 10 IU., Biovendor, Asheville, NC) and with human chorionic gonadotrophin 48 h later if collecting eggs/zygotes (hCG, 10 IU., Sigma-Aldrich, St. Louis, MO). Cumulus-enclosed, GV oocytes (COCs) were obtained 40 h after the PMSG injection following removal and mincing of the ovaries and piercing the large antral follicles; MII eggs were recovered from the oviducts 12 h after the hCG injection. GV oocytes and eggs were handled in HEPES-buffered Tyrode's lactate solution (TL-HEPES). To procure *in vivo*

zygotes, after the hCG injection, females were paired with males overnight. A vaginal plug 14 h after hCG was evidence of successful mating. Putative zygotes were collected from the oviducts of females 20h post-hCG administration and briefly incubated with hyaluronidase and transferred into micro drops of KSOM (MilliporeSigma) covered with light mineral oil (Fisher Scientific, Hampton, NH) in an incubator under a humidified atmosphere in air containing 5% CO_2 and at 37°C. PN formation was evaluated at 24 h post-hCG and cleavage to 2C at 40 h.

For flushing *in vivo*-produced embryos from the oviduct, a 32 gauge needle (the end cut and ground to blunt the tip) is attached to a 1 ml syringe filled with media. The embryos were flushed at 36 h (2C) and 60 h (8C) post-ovulation. Flushed embryos were cultured as mentioned above.

Zygotes were also produced by *in vitro* fertilization (IVF), and egg collection was performed as described above. For IVF, eggs were placed in 90 μL drops of Toyoda-Yokoyama-Hosi medium (TYH;[75]) supplemented with 4 mg mL^{-1} of BSA (TYH-BSA; Sigma-Aldrich) covered with mineral oil and incubated under standard conditions. Sperm were recovered from 2- to 6-month-old male's cauda epididymis and placed in 1 mL TYH-BSA and allowed to swim out for 10 min. Additional sperm incubation, capacitation, and insemination were performed as described[76,77]. After 4 h, eggs were gently pipetted, washed, and incubated for 20 h in fresh TYH-BSA micro drops covered with mineral oil. After this time, zygotes were washed, placed into KSOM medium (MilliporeSigma), and cultured in standard conditions for variable intervals according to the experimental design.

Zygotes from all groups were washed and transferred to KSOM micro drops covered with mineral oil and cultured for 24-96 h according to experimental design. Their progression through development was evaluated every 24 h and until 120 h post-hCG, and embryos were scored (2-cell (2C), 4-cell (4C), 8-cell (8C) embryo, morula, or blastocysts (BLs). To assess cell numbers, BLs were fixed in 4% paraformaldehyde (PFA), stained with 1% (w/v) Hoechst 33342 (Thermo Fisher), and mounted on slides under coverslips using 1% glycerol. The cell counts were performed in BLs at 400x under an epifluorescence microscope (Eclipse TE300, Nikon, Japan). The culture media for rescue experiments was supplemented with 10μM $ZnCl_2$, or 10mM $MgSO_4{\cdot}7H_2O$ or their combination, at the 2C-, 4C-, or 8C stages. Embryo development and cell numbers were scored or counted as described. Eggs and embryos used for RNA isolation and sequencing studies, see procedures below, were collected following identical procedures and timelines.

For the outgrowth assay, BLs were cultured as mentioned in Miao et al. 2020[78]. Briefly, BLs were cultured for 3 days in Dulbecco's modified Eagle's medium (DMEM, Lonza, MD, USA), supplemented with 10% fetal bovine serum (FBS, R&D systems, Minneapolis, MN) and 1X Glutamax (Fisher scientific) on glass slides, and several different external concentrations of Mg^{2+} with the purpose to establish the need of Mg^{2+} post-BL stage. Individual outgrowths were imaged and manually marked the boundaries of ICM and TE cells.

Intracellular divalent cation imaging—Imaging for divalent cations in eggs and embryos was done as reported by our group[39] or following procedures published by others.[7,79] Eggs were pre-loaded with 1.25 μM Ca^{2+} sensitive dye Fura-2-acetoxymethyl ester (Fura 2-AM; Invitrogen, Waltham, MA) in the presence of 0.02% pluronic acid (Thermo Fisher) for 10 min. Intracellular Zn^{2+} levels were measured using 1.25 μM FluoZin™-3 AM and loaded for 20 min (Invitrogen), while Mg^{2+} was assessed using 0.6 μM Mag-Fura-2 AM (Invitrogen) loaded for 5 min following the above procedures. The dye-loaded eggs were placed onto the bottom of glass-bottom dishes and given time to settle (Mat-Tek Corp., Ashland, MA). A group of eggs was monitored simultaneously using an inverted microscope (Nikon, Melville, NY) outfitted for fluorescence measurements. Fura-2 and Mag-Fura-2 were excited at 340 and 380 nm wavelengths, whereas FluoZin was at 480 nm, every 20s, and the light source was a 75-W Xenon arc lamp (Ludl Electronic Products Ltd., Hawthorne, NY). A cooled Photometrics SenSys CCD camera (Roper Scientific, Artisan Technology Group, Champaign, IL) collected the emitted light above 510 nm, and images were captured and processed using the Nikon NIS-Elements software.

Data analyses and plotting were performed using GraphPad Prism (GraphPad Software, San Diego, CA). F340/380 ratios were used to compare basal Ca^{2+} and Sr^{2+} concentrations among embryos from different genetic lines. Estimation of Zn^{2+} and Mg^{2+} levels between strains was carried out following normalization using the initial values of each recorded egg/embryo (F_0), F_1/F_0 (Zn^{2+}), or the following the formula $(F_0\text{-}F_{max})/(F_{max}\text{-}F_{min})$ (Mg^{2+}).[79] The duration of the monitoring period depended on the experimental design but was as brief as 15 min and as long as 120 min for fertilization-induced responses. To assess sperm-induced Ca^{2+} oscillations, we used ZP-free eggs that reduced the time to fertilization. The ZP was removed following a short exposure to acid Tyrode's solution (pH=2.5). For these experiments, Fura 2-AM staining was as above, but Cell-Tak was used to coat the monitoring dishes and hold eggs in place during monitoring (Corning, Corning. NY). Sperm were added to final concentrations of ~$0.5x10^5$ mL^{-1} a few min after monitoring basal Ca^{2+}.

To compare intracellular Mg^{2+} concentrations among different embryo stages, we used two approaches to obtain embryos. At first, we collected *in vivo* fertilized embryos, cultured them for varied amounts of time until the 2, 4, and 8C stages, and monitored along freshly collected MIIs, which served as controls. In the second approach, *in vivo*, fertilized embryos following mating females at different times were flushed together, and we measured all embryo stages simultaneously, including MII eggs. Both approaches yielded the same results. Mg^{2+} was measured with the methods described above and in single blastomeres; blastomeres were isolated from others by 1 h incubation in Ca^{2+}-free media supplemented with 500 μM of EDTA. Previously, the ZP was removed using Tyrode's acid.

Sperm analysis—Spermatozoa of *Trpm7*$^{fl/fl}$ and *Trpm7*-Sp cKO were examined and compared following standard methods.[80] Sperm concentration and morphology were evaluated in non-capacitated (NCAP) spermatozoa fixed after swimming out. After washing, they were resuspended in PBS, and 200 were analyzed per sample using contrast-phase microscopy at 400X. Sperm motility was determined in NCAP and in capacitated spermatozoa (CAP) by loading 35 μL into a pre-warmed chamber slide (Leja, 100 μm in depth) at 37 °C. CEROS computer-assisted sperm analysis system, CASA (Hamilton

Thorne Research, Beverly, MA), was used with the default setting to analyze at least five microscopy fields. The acrosome status in NCAP and CAP sperm was examined using fixed samples spread on poly-L-lysine treated slides and air-dried. Following permeabilization and washes, sperm were incubated with Alexa Fluor 488-conjugated PNA lectin (Invitrogen) 1:100 in PBS at RT and protected from light for one h. Slides were treated with mounting medium (Vectashield, Vector Laboratories, Newark, CA) and permanently mounted with coverslips sealed with nail polish.

Production of anti-TRPM7 monoclonal antibody—A monoclonal antibody, DA5C7-TRPM7, was produced in-house and generated against a bacterial fusion protein corresponding to the C-term portion of the cytoplasmic domain of mTRPM7 (amino acids 1159-1413). We followed standard hybridoma procedures and techniques described in the noted reference[81]. Briefly, BalbC mice (Jackson Laboratories) were immunized with the TRPM7 protein. Following the production of hybridomas via electrofusion, these were screened by immunofluorescence using fixed *Xenopus*-XTC cells expressing *mTrpm7-GFP* (a kind gift from Dr. V. Chubanov, Ludwig-Maximilians-University of Munich, Germany). After the identification of candidate hybridomas, cells were subcloned and frozen. Identification and validation of the DA5C7-TRPM7 antibody were performed by Western blotting and immunofluorescence on XTC cells, followed by additional testing on mouse eggs and sperm (WT, *Trpm7*-Oo cKO, and *Trpm7*-Sp cKO). The clones producing the DA5C7-TRPM7 antibody were further expanded and stored for future production.

Western blotting—Cell lysates from GV oocytes, MII eggs, and embryos (n=50 per lane and sample) from $Trpm7^{fl/fl}$ and *Trpm7*-null females and crosses were prepared by adding 2X-Laemmli sample buffer immediately after collection and frozen until use. Sperm proteins were extracted as described[80]. Briefly, after swim-out, the sperm were centrifuged and washed in cold 1X PBS, centrifuged, resuspended in SDS-Laemmli buffer supplemented with β-mercaptoethanol, boiled for 4 min, and frozen until use. Whole tissue lysates were prepared as published by us[82]. Upon thawing, samples were boiled, mixed well, separated on 6% SDS-PAGE gels, and transferred for 2 h to PVDF membranes (Millipore Sigma). After blocking with 5% fat-free milk in TPBS, the membranes were incubated overnight at 4°C with a monoclonal DA5C7-TRPM7 antibody. A goat anti-mouse IgG (Invitrogen) was used as the secondary antibody. After thoroughly washing the membranes, chemiluminescence detection was accomplished using ECL Prime (Sigma-Aldrich) and 1–5 min exposure to maximum sensitivity Kodak Biomax film (VWR, Radnor, PA), which was developed in an X-ray film processor (Optimax Protech Processor Technology, Germany). Noteworthy, to avoid substrate competition between gametes and embryos with widely different reactivities, after exposure to the secondary antibody, the membrane was divided into individual strips cut along vertical lines corresponding to the width of each well, incubated separately for 1 min in aliquots of an equal volume of the same ECL Prime master mix. The strips were reassembled as loaded in the gel and simultaneously exposed to the film. This approach enhanced signal detection in all samples and stages. Broad-range pre-stained SDS–PAGE molecular weight markers (Bio-Rad) were run in parallel to estimate the molecular weight of the immunoreactive bands. These membranes were stripped at 50°C for 30 min (62.5 mM Tris, 2% SDS, and 100 mM 2-beta mercaptoethanol) and re-probed

with anti-α-tubulin monoclonal antibody (Sigma-Aldrich, T9026, 1:1000), which was used as a loading control and to normalize the quantification procedures.

Preparation and microinjection of mRNA—pcDNA*6*-D1ER-KDEL, pcDNA6-*mTrpm7*^{wt}*-Gfp,* pcDNA6-*mTrpm7*^{K1646R}*-Gfp,* pcDNA6-*mTrpm7*^{P1040R}*-Gfp, and* pcDNA6-*mTrpm7*^{1570Stop}*-Gfp* and were linearized with the restriction enzyme *Pme1* and *in vitro* transcribed using the T7 mMESSAGE mMACHINE kit (Invitrogen) following procedures described in our previous studies.[39] A poly(A) tail was added to the *in vitro* synthesized RNA (mRNA) using a Tailing Kit, followed by quantification and dilution in nuclease-free water and stored at −80°C until use. Before microinjection, *mTrpm7-Gfp* mRNA was diluted in nuclease-free water to 1.0 μg/μl, heated at 95°C for 3 min, and centrifuged at 13,400×*g* for 10 min at 4°C. Cytoplasmic injection of mRNA was performed under a microscope equipped with micromanipulators (Narishige, Japan). The ZP and PM of zygotes were breached by applying small pulses generated by the piezo micromanipulator (Primetech, Ibaraki, Japan). Injections were performed with ICSI pipettes[83] but with a tip diameter of ~1 μm, and injected zygotes were monitored for development until the BL stage.

Immunostaining of gametes and embryos and confocal microscopy—Immunostaining was performed according to published protocols.[74,84] Oocytes, eggs, and embryos were fixed with 4% (w/v) PFA in phosphate-buffered saline (PBS) for 20 min at RT and permeabilized for 60 min with 0.2% (v/v) Triton X-100 in PBS. Sperm were handled as above, but upon fixation, were placed onto poly-lysine coated coverslips and air dried for 15 min. The samples were blocked for 45 min in a buffer containing 0.2% (w/v) skim milk, 2% (v/v) fetal bovine serum, 1% (w/v) bovine serum albumin, 0.1% (v/v) TritonX-100, 0.75% (w/v) glycine in PBS. Gametes and embryos were incubated overnight at 4°C with mouse anti-TRPM7 antibody (1:1000) diluted in blocking buffer, followed by washes in 3X blocking buffer for 10 min, incubation at RT for 30 min with the secondary antibody Alexa Fluor 488 goat anti-mouse IgG (H + L) (1:400; (Invitrogen) diluted in blocking buffer that contained rhodamine-Phalloidin (1:100, Invitrogen) and Hoechst 33342 (1:100, Thermo Fisher). The secondary antibody mixture for sperm included Lectin-PNA (Invitrogen, L32458, 1:100) instead of rhodamine phalloidin, was incubated for one h and followed by mounting on coverslips using Vectashield mounting solution (Vector Laboratories). For lipid vesicle staining, fixed and permeabilized BLs were incubated with 10 μg/ml BODIPY (Invitrogen) for 30 min. For the detection of apoptotic cells, we used the TUNEL Assay Apoptosis Detection Kit (30074, Biotium) following the manufacturer's protocol and instructions. Briefly, fixed and permeabilized BLs were incubated with the TUNEL reaction buffer and TdT enzyme for 1 h at 37°C, washed 3X 5 min followed by 10 min staining with Hoechst 33342 (1:100, Thermo Fisher). A laser-scanning confocal microscope (Nikon A1 Resonant Confocal with six-color TIRF) fitted with a 63X 1.4 NA oil-immersion objective lens was used to visualize the fluorescence signals.

Determination of mitochondrial membrane potential—To assess the status of the mitochondria as an estimation of the embryos' oxidative stress, we evaluated their membrane potential using the JC-1 assay (Abcam, Cambridge, UK). The procedure was carried out as per the manufacturer's instructions. Briefly, eggs and embryos were incubated

with JC-1 (10 μM) in KSOM for 30 min at 37°C in the dark. Eggs and embryos were then washed and imaged immediately using confocal microscopy, as described above. The red-to-green fluorescence ratio was averaged for ten z-sections and quantified using ImageJ.

Egg and embryo RNA isolation and sequencing—RNA was sequenced from eggs or embryos from zygotes to BLs. Four biological replicates at each stage for each group were sequenced. Each biological replicate consisted of five eggs or embryos. Following collection as described, eggs and embryos were washed in sterile PBS and snap-frozen on dry ice. RNA was prepared using the SMART-Seq v4 Ultra Low Input RNA Kit (Takara Bio, Japan), and cDNA was purified using the Agencourt AMPure XP kit (Beckman Coulter). RNA quality and yield were measured using the Agilent 2100 Bioanalyzer (Agilent Technologies). Library preparation was carried out on 100-150 pg amplified cDNA using the Illumina DNA Prep kit (Illumina, San Diego, CA). Sequencing was performed on a NovaSeq 6000 Sequencing System (Illumina).

RNA-seq data processing and analysis—Adapter and low-quality tails were removed from sequenced reads using Cutadapt (v3.7)[85] prior to alignment to the reference genome using STAR (v2.6.0c).[86] RNA abundance was quantified using uniquely mapped reads only with feature Counts (v1.6.3)[87] and GENCODE mouse reference GRCm38 vM17. For each set of replicates, the sample with the lowest number of gene-associated reads was removed from downstream analysis. The sequencing data generated in this study have been deposited in the Gene Expression Omnibus database and will be publicly available as of the date of publication.

Differential expression between experimental groups was carried out using DESeq2 (v1.34.0),[88]. Hierarchical clustering was performed using the R function Hclust with Euclidean distances between variance-stabilizing transformed count data. Visualization was carried out by transforming this data to z-scores within comparison sets prior to heatmap generation. DEGs were analyzed using Ingenuity Pathway Analysis (Qiagen, Germantown, MD). Canonical pathways and upstream regulators were filtered for $p < 0.05$ and >2 molecules.

QUANTIFICATION AND STATISTICAL ANALYSIS

Comparisons for statistical significance of experimental values between treatments and experiments were performed with at least three experiments on different batches of gametes or embryos. Data were compared using SPSS Statistics (v.20) or GraphPad software packages, including *Student's t-test,* One-Way ANOVA followed by multiple comparisons Tukey post-hoc test, or Fisher's exact Chi-Square test, depending on the experiment and type of data analyzed. In addition, the number of replicates and statistical analyses used are indicated in the figure and table legends. The numerical data are presented as mean ± s.d. Significant differences were considered when *$p < 0.05$, **$p < 0.01$, ***$p < 0.001$, or ****$p < 0.0001$.

Supplementary Material

Refer to Web version on PubMed Central for supplementary material.

ACKNOWLEDGMENTS

We thank Fissore lab members Dr. Hiroki Akizawa and Ms. Changli He for their valuable discussions and contributions in maintaining the mouse lines. We also thank Dr. Visconti's lab for assistance with the analysis of sperm parameters using CASA. R.A.F. discloses support for this research from NIH (RO1 HD092499). C.J.W. discloses support for this research from the Intramural Research Program of the National Institutes of Health, National Institute of Environmental Health Sciences (1ZIAES102405). D.A. discloses support for this research from NIH R24 OD021485 and R01 DE016289. I.C.'s contributions were supported in part by the NIH (RO1 HD092499) and FONDECYT 1221308.

REFERENCES

1. Komiya Y, Mandrekar N, Sato A, Dawid IB, and Habas R (2014). Custos controls β-catenin to regulate head development during vertebrate embryogenesis. Proc. Natl. Acad. Sci. USA 111, 13099–13104. [PubMed: 25157132]
2. Krauchunas AR, and Wolfner MF (2013). Molecular changes during egg activation. Curr. Top. Dev. Biol 102, 267–292. [PubMed: 23287037]
3. Stein P, Savy V, Williams AM, and Williams CJ (2020). Modulators of calcium signalling at fertilization. Open Biol. 10, 200118. [PubMed: 32673518]
4. Wozniak KL, and Carlson AE (2020). Ion channels and signaling pathways used in the fast polyspermy block. Mol. Reprod. Dev 87, 350–357. [PubMed: 31087507]
5. Stricker SA (1999). Comparative biology of calcium signaling during fertilization and egg activation in animals. Dev. Biol 211, 157–176. [PubMed: 10395780]
6. Wakai T, and Fissore RA (2019). Constitutive IP(3)R1-mediated Ca(2+) release reduces Ca(2+) store content and stimulates mitochondrial metabolism in mouse GV oocytes. J. Cell Sci 132, jcs225441. [PubMed: 30659110]
7. Kim AM, Vogt S, O'Halloran TV, and Woodruff TK (2010). Zinc availability regulates exit from meiosis in maturing mammalian oocytes. Nat. Chem. Biol 6, 674–681. [PubMed: 20693991]
8. Kim AM, Bernhardt ML, Kong BY, Ahn RW, Vogt S, Woodruff TK, and O'Halloran TV (2011). Zinc sparks are triggered by fertilization and facilitate cell cycle resumption in mammalian eggs. ACS Chem. Biol 6, 716–723. [PubMed: 21526836]
9. Suzuki T, Yoshida N, Suzuki E, Okuda E, and Perry ACF (2010). Full-term mouse development by abolishing Zn2+-dependent metaphase II arrest without Ca2+ release. Development 137, 2659–2669. [PubMed: 20591924]
10. Burkart AD, Xiong B, Baibakov B, Jiménez-Movilla M, and Dean J (2012). Ovastacin, a cortical granule protease, cleaves ZP2 in the zona pellucida to prevent polyspermy. J. Cell Biol 197, 37–44. [PubMed: 22472438]
11. Tokuhiro K, and Dean J (2018). Glycan-Independent Gamete Recognition Triggers Egg Zinc Sparks and ZP2 Cleavage to Prevent Polyspermy. Dev. Cell 46, 627–640.e5. [PubMed: 30122633]
12. Bernhardt ML, Stein P, Carvacho I, Krapp C, Ardestani G, Mehregan A, Umbach DM, Bartolomei MS, Fissore RA, and Williams CJ (2018). TRPM7 and Ca(V)3.2 channels mediate Ca(2+) influx required for egg activation at fertilization. Proc. Natl. Acad. Sci. USA 115. E10370–e10378. [PubMed: 30322909]
13. Ozil JP, Sainte-Beuve T, and Banrezes B (2017). [Mg(2+)](o)/[Ca(2+)](o) determines Ca(2+) response at fertilization: tuning of adult phenotype? Reproduction 154, 675–693. [PubMed: 28851827]
14. Wakai T, Vanderheyden V, and Fissore RA (2011). Ca2+ signaling during mammalian fertilization: requirements, players, and adaptations. Cold Spring Harbor Perspect. Biol 3, a006767.
15. Carvacho I, Ardestani G, Lee HC, McGarvey K, Fissore RA, and Lykke-Hartmann K (2016). TRPM7-like channels are functionally expressed in oocytes and modulate post-fertilization embryo development in mouse. Sci. Rep 6, 34236. [PubMed: 27681336]
16. Peres A. (1987). The calcium current of mouse egg measured in physiological calcium and temperature conditions. J. Physiol 391, 573–588. [PubMed: 2451013]

17. Bernhardt ML, Zhang Y, Erxleben CF, Padilla-Banks E, McDonough CE, Miao YL, Armstrong DL, and Williams CJ (2015). CaV3.2 T-type channels mediate Ca^{2+} entry during oocyte maturation and following fertilization. J. Cell Sci 128, 4442–4452. [PubMed: 26483387]
18. Carvacho I, Lee HC, Fissore RA, and Clapham DE (2013). TRPV3 channels mediate strontium-induced mouse-egg activation. Cell Rep. 5, 1375–1386. [PubMed: 24316078]
19. Bernhardt ML, Padilla-Banks E, Stein P, Zhang Y, and Williams CJ (2017). Store-operated Ca(2+) entry is not required for fertilization-induced Ca(2+) signaling in mouse eggs. Cell Calcium 65, 63–72. [PubMed: 28222911]
20. Mehregan A, Ardestani G, Akizawa H, Carvacho I, and Fissore R (2021). Deletion of TRPV3 and CaV3.2 T-type channels in mice undermines fertility and Ca2+ homeostasis in oocytes and eggs. J. Cell Sci 134, jcs257956. [PubMed: 34313315]
21. Jin J, Desai BN, Navarro B, Donovan A, Andrews NC, and Clapham DE (2008). Deletion of Trpm7 disrupts embryonic development and thymopoiesis without altering Mg2+ homeostasis. Science 322, 756–760. [PubMed: 18974357]
22. Lichten LA, and Cousins RJ (2009). Mammalian zinc transporters: nutritional and physiologic regulation. Annu. Rev. Nutr 29, 153–176. [PubMed: 19400752]
23. Kambe T, Tsuji T, Hashimoto A, and Itsumura N (2015). The Physiological, Biochemical, and Molecular Roles of Zinc Transporters in Zinc Homeostasis and Metabolism. Physiol. Rev 95, 749–784. [PubMed: 26084690]
24. Kong BY, Duncan FE, Que EL, Kim AM, O'Halloran TV, and Woodruff TK (2014). Maternally-derived zinc transporters ZIP6 and ZIP10 drive the mammalian oocyte-to-egg transition. Mol. Hum. Reprod 20, 1077–1089. [PubMed: 25143461]
25. Dufner-Beattie J, Weaver BP, Geiser J, Bilgen M, Larson M, Xu W, and Andrews GK (2007). The mouse acrodermatitis enteropathica gene Slc39a4 (Zip4) is essential for early development and heterozygosity causes hypersensitivity to zinc deficiency. Hum. Mol. Genet 16, 1391–1399. [PubMed: 17483098]
26. Hara T, Yoshigai E, Ohashi T, and Fukada T (2022). Zinc transporters as potential therapeutic targets: An updated review. J. Pharmacol. Sci 148, 221–228. [PubMed: 35063137]
27. Romani AMP (2011). Cellular magnesium homeostasis. Arch. Biochem. Biophys 512, 1–23. [PubMed: 21640700]
28. Chubanov V, Ferioli S, Wisnowsky A, Simmons DG, Leitzinger C, Einer C, Jonas W, Shymkiv Y, Bartsch H, Braun A, et al. (2016). Epithelial magnesium transport by TRPM6 is essential for prenatal development and adult survival. Elife 5, e20914. [PubMed: 27991852]
29. Jin J, Wu LJ, Jun J, Cheng X, Xu H, Andrews NC, and Clapham DE (2012). The channel kinase, TRPM7, is required for early embryonic development. Proc. Natl. Acad. Sci. USA 109, E225–E233. [PubMed: 22203997]
30. Schütz A, Richter C, Weissgerber P, Tsvilovskyy V, Hesse M, Ottenheijm R, Zimmermann F, Buchholz S, Medert R, Dlugosz S, et al. (2021). Trophectoderm cell failure leads to peri-implantation lethality in Trpm7-deficient mouse embryos. Cell Rep. 37, 109851. [PubMed: 34686339]
31. Nadler MJ, Hermosura MC, Inabe K, Perraud AL, Zhu Q, Stokes AJ, Kurosaki T, Kinet JP, Penner R, Scharenberg AM, and Fleig A (2001). LTRPC7 is a Mg.ATP-regulated divalent cation channel required for cell viability. Nature 411, 590–595. [PubMed: 11385574]
32. Monteilh-Zoller MK, Hermosura MC, Nadler MJS, Scharenberg AM, Penner R, and Fleig A (2003). TRPM7 provides an ion channel mechanism for cellular entry of trace metal ions. J. Gen. Physiol 121, 49–60. [PubMed: 12508053]
33. Li M, Jiang J, and Yue L (2006). Functional characterization of homo- and heteromeric channel kinases TRPM6 and TRPM7. J. Gen. Physiol 127, 525–537. [PubMed: 16636202]
34. Schmitz C, Perraud AL, Johnson CO, Inabe K, Smith MK, Penner R, Kurosaki T, Fleig A, and Scharenberg AM (2003). Regulation of vertebrate cellular Mg2+ homeostasis by TRPM7. Cell 114, 191–200. [PubMed: 12887921]
35. Krapivinsky G, Krapivinsky L, Manasian Y, and Clapham DE (2014). The TRPM7 chanzyme is cleaved to release a chromatin-modifying kinase. Cell 157, 1061–1072. [PubMed: 24855944]

36. Wu D, and Dean J (2020). Maternal factors regulating preimplantation development in mice. Curr. Top. Dev. Biol 140, 317–340. [PubMed: 32591079]
37. Inselman AL, Nakamura N, Brown PR, Willis WD, Goulding EH, and Eddy EM (2010). Heat shock protein 2 promoter drives Cre expression in spermatocytes of transgenic mice. Genesis 48, 114–120. [PubMed: 20027617]
38. Govin J, Caron C, Escoffier E, Ferro M, Kuhn L, Rousseaux S, Eddy EM, Garin J, and Khochbin S (2006). Post-meiotic shifts in HSPA2/HSP70.2 chaperone activity during mouse spermatogenesis. J. Biol. Chem 281, 37888–37892. [PubMed: 17035236]
39. Ardestani G, Mehregan A, Fleig A, Horgen FD, Carvacho I, and Fissore RA (2020). Divalent cation influx and calcium homeostasis in germinal vesicle mouse oocytes. Cell Calcium 87, 102181. [PubMed: 32097818]
40. Cai N, Bai Z, Nanda V, and Runnels LW (2017). Mass Spectrometric Analysis of TRPM6 and TRPM7 Phosphorylation Reveals Regulatory Mechanisms of the Channel-Kinases. Sci. Rep 7, 42739. [PubMed: 28220887]
41. Desai BN, Krapivinsky G, Navarro B, Krapivinsky L, Carter BC, Febvay S, Delling M, Penumaka A, Ramsey IS, Manasian Y, and Clapham DE (2012). Cleavage of TRPM7 releases the kinase domain from the ion channel and regulates its participation in Fas-induced apoptosis. Dev. Cell 22, 1149–1162. [PubMed: 22698280]
42. Abiria SA, Krapivinsky G, Sah R, Santa-Cruz AG, Chaudhuri D, Zhang J, Adstamongkonkul P, DeCaen PG, and Clapham DE (2017). TRPM7 senses oxidative stress to release Zn(2+) from unique intracellular vesicles. Proc. Natl. Acad. Sci. USA 114. E6079–e6088. [PubMed: 28696294]
43. Palmer AE, Jin C, Reed JC, and Tsien RY (2004). Bcl-2-mediated alterations in endoplasmic reticulum Ca2+ analyzed with an improved genetically encoded fluorescent sensor. Proc. Natl. Acad. Sci. USA 101, 17404–17409. [PubMed: 15585581]
44. Wathlet S, Adriaenssens T, Segers I, Verheyen G, Van de Velde H, Coucke W, Ron El R, Devroey P, and Smitz J (2011). Cumulus cell gene expression predicts better cleavage-stage embryo or blastocyst development and pregnancy for ICSI patients. Hum. Reprod 26, 1035–1051. [PubMed: 21372047]
45. Brinster RL (1967). PROTEIN CONTENT OF THE MOUSE EMBRYO DURING THE FIRST FIVE DAYS OF DEVELOPMENT. Reproduction 13, 413–420.
46. Zeng F, Baldwin DA, and Schultz RM (2004). Transcript profiling during preimplantation mouse development. Dev. Biol 272, 483–496. [PubMed: 15282163]
47. Park SJ, Shirahige K, Ohsugi M, and Nakai K (2015). DBTMEE: a database of transcriptome in mouse early embryos. Nucleic Acids Res. 43, D771–D776. [PubMed: 25336621]
48. Chubanov V, Schlingmann KP, Wäring J, Heinzinger J, Kaske S, Waldegger S, Mederos y Schnitzler M, and Gudermann T (2007). Hypomagnesemia with secondary hypocalcemia due to a missense mutation in the putative pore-forming region of TRPM6. J. Biol. Chem 282, 7656–7667. [PubMed: 17197439]
49. Ryazanova LV, Hu Z, Suzuki S, Chubanov V, Fleig A, and Ryazanov AG (2014). Elucidating the role of the TRPM7 alpha-kinase: TRPM7 kinase inactivation leads to magnesium deprivation resistance phenotype in mice. Sci. Rep 4, 7599. [PubMed: 25534891]
50. Ryazanova LV, Rondon LJ, Zierler S, Hu Z, Galli J, Yamaguchi TP, Mazur A, Fleig A, and Ryazanov AG (2010). TRPM7 is essential for Mg(2+) homeostasis in mammals. Nat. Commun 1, 109. [PubMed: 21045827]
51. Sahni J, Tamura R, Sweet IR, and Scharenberg AM (2010). TRPM7 regulates quiescent/proliferative metabolic transitions in lymphocytes. Cell Cycle 9, 3565–3574. [PubMed: 20724843]
52. Hanano T, Hara Y, Shi J, Morita H, Umebayashi C, Mori E, Sumimoto H, Ito Y, Mori Y, and Inoue R (2004). Involvement of TRPM7 in cell growth as a spontaneously activated Ca2+ entry pathway in human retinoblastoma cells. J. Pharmacol. Sci 95, 403–419. [PubMed: 15286426]
53. Middelbeek J, Kuipers AJ, Henneman L, Visser D, Eidhof I, van Horssen R, Wieringa B, Canisius SV, Zwart W, Wessels LF, et al. (2012). TRPM7 is required for breast tumor cell metastasis. Cancer Res. 72, 4250–4261. [PubMed: 22871386]
54. Mittermeier L, Demirkhanyan L, Stadlbauer B, Breit A, Recordati C, Hilgendorff A, Matsushita M, Braun A, Simmons DG, Zakharian E, et al. (2019). TRPM7 is the central gatekeeper of

intestinal mineral absorption essential for postnatal survival. Proc. Natl. Acad. Sci. USA 116, 4706–4715. [PubMed: 30770447]

55. Elizondo MR, Arduini BL, Paulsen J, MacDonald EL, Sabel JL, Henion PD, Cornell RA, and Parichy DM (2005). Defective skeleto-genesis with kidney stone formation in dwarf zebrafish mutant for trpm7. Curr. Biol 15, 667–671. [PubMed: 15823540]
56. Liu W, Su LT, Khadka DK, Mezzacappa C, Komiya Y, Sato A, Habas R, and Runnels LW (2011). TRPM7 regulates gastrulation during vertebrate embryogenesis. Dev. Biol 350, 348–357. [PubMed: 21145885]
57. Franken GAC, Huynen MA, Martínez-Cruz LA, Bindels RJM, and de Baaij JHF (2022). Structural and functional comparison of magnesium transporters throughout evolution. Cell. Mol. Life Sci 79, 418. [PubMed: 35819535]
58. Jaffe LA, and Egbert JR (2017). Regulation of Mammalian Oocyte Meiosis by Intercellular Communication Within the Ovarian Follicle. Annu. Rev. Physiol 79, 237–260. [PubMed: 27860834]
59. Mishieva N, Martazanova B, Bogatyreva K, Korolkova A, Kirillova A, Veyukova M, Burmenskaya O, Abubakirov A, and Sukhikh GT (2020). Cumulus cell gene expression in luteal-phase-derived oocytes after double stimulation in one menstrual cycle. Reprod. Biomed. Online 41, 518–526. [PubMed: 32593508]
60. Wathlet S, Adriaenssens T, Segers I, Verheyen G, Janssens R, Coucke W, Devroey P, and Smitz J (2012). New candidate genes to predict pregnancy outcome in single embryo transfer cycles when using cumulus cell gene expression. Fertil. Steril 98, 432–439. [PubMed: 22633264]
61. Kunert-Keil C, Bisping F, Krüger J, and Brinkmeier H (2006). Tissue-specific expression of TRP channel genes in the mouse and its variation in three different mouse strains. BMC Genom. 7, 159.
62. Runnels LW, Yue L, Clapham DE, and TRP-PLIK. (2001). a bifunctional protein with kinase and ion channel activities. Science 291, 1043–1047. [PubMed: 11161216]
63. Clark K, Middelbeek J, Dorovkov MV, Figdor CG, Ryazanov AG, Lasonder E, and van Leeuwen FN (2008). The alpha-kinases TRPM6 and TRPM7, but not eEF-2 kinase, phosphorylate the assembly domain of myosin IIA, IIB and IIC. FEBS Lett. 582, 2993–2997. [PubMed: 18675813]
64. Johnson MH, and Ziomek CA (1983). Cell interactions influence the fate of mouse blastomeres undergoing the transition from the 16- to the 32-cell stage. Dev. Biol 95, 211–218. [PubMed: 6825925]
65. Zhu D, Su Y, Young ML, Ma J, Zheng Y, and Tang L (2017). Biological Responses and Mechanisms of Human Bone Marrow Mesenchymal Stem Cells to Zn and Mg Biomaterials. ACS Appl. Mater. Interfaces 9, 27453–27461. [PubMed: 28787130]
66. Rivera RM, and Ross JW (2013). Epigenetics in fertilization and preimplantation embryo development. Prog. Biophys. Mol. Biol 113, 423–432. [PubMed: 23454467]
67. Messerschmidt DM, Knowles BB, and Solter D (2014). DNA methylation dynamics during epigenetic reprogramming in the germline and preimplantation embryos. Genes Dev. 28, 812–828. [PubMed: 24736841]
68. Xu J, Shu Y, Yao G, Zhang Y, Niu W, Zhang Y, Ma X, Jin H, Zhang F, Shi S, et al. (2021). Parental methylome reprogramming in human uniparental blastocysts reveals germline memory transition. Genome Res. 31, 1519–1530. [PubMed: 34330789]
69. de Baaij JHF (2015). The art of magnesium transport. Magnes. Res 28, 85–91. [PubMed: 26446763]
70. Trapani V, and Wolf FI (2019). Dysregulation of Mg(2+) homeostasis contributes to acquisition of cancer hallmarks. Cell Calcium 83, 102078. [PubMed: 31493712]
71. Wolf FI, Maier JAM, Nasulewicz A, Feillet-Coudray C, Simonacci M, Mazur A, and Cittadini A (2007). Magnesium and neoplasia: from carcinogenesis to tumor growth and progression or treatment. Arch. Biochem. Biophys 458, 24–32. [PubMed: 16564020]
72. Sun J, Wu X, Xu X, Jin L, Han N, and Zhou R (2012). A comparison of epidural magnesium and/or morphine with bupivacaine for postoperative analgesia after cesarean section. Int. J. Obstet. Anesth 21, 310–316. [PubMed: 22858044]

73. Mazur A, Maier JAM, Rock E, Gueux E, Nowacki W, and Rayssiguier Y (2007). Magnesium and the inflammatory response: potential physiopathological implications. Arch. Biochem. Biophys 458, 48–56. [PubMed: 16712775]
74. Akizawa H, Saito S, Kohri N, Furukawa E, Hayashi Y, Bai H, Nagano M, Yanagawa Y, Tsukahara H, Takahashi M, et al. (2021). Deciphering two rounds of cell lineage segregations during bovine preimplantation development. Faseb. J 35, e21904. [PubMed: 34569650]
75. Y T. (1971). Studies on the Fertilization of Mouse Eggs in Vitro.
76. Ducibella T, and Matson S (2007). Secretory mechanisms and Ca2+ signaling in gametes: similarities to regulated neuroendocrine secretion in somatic cells and involvement in emerging pathologies. Endocr. Pathol 18, 191–203. [PubMed: 18247164]
77. Navarrete FA, Aguila L, Martin-Hidalgo D, Tourzani DA, Luque GM, Ardestani G, Garcia-Vazquez FA, Levin LR, Buck J, Darszon A, et al. (2019). Transient Sperm Starvation Improves the Outcome of Assisted Reproductive Technologies. Front. Cell Dev. Biol 7, 262. [PubMed: 31750304]
78. Miao X, Sun T, Golan M, Mager J, and Cui W (2020). Loss of POLR1D results in embryonic lethality prior to blastocyst formation in mice. Mol. Reprod. Dev 87, 1152–1158. [PubMed: 33022126]
79. Tashiro M, Inoue H, and Konishi M (2014). Physiological pathway of magnesium influx in rat ventricular myocytes. Biophys. J 107, 2049–2058. [PubMed: 25418090]
80. Tourzani DA, Paudel B, Miranda PV, Visconti PE, and Gervasi MG (2018). Changes in Protein O-GlcNAcylation During Mouse Epididymal Sperm Maturation. Front. Cell Dev. Biol 6, 60. [PubMed: 29942801]
81. Horr B, Kurtz R, Pandey A, Hoffstrom BG, Schock E, LaBonne C, and Alfandari D (2023). Production and characterization of monoclonal antibodies to Xenopus proteins. Development 150, dev201309. [PubMed: 36789951]
82. Wu H, He CL, Jehn B, Black SJ, and Fissore RA (1998). Partial characterization of the calcium-releasing activity of porcine sperm cytosolic extracts. Dev. Biol 203, 369–381. [PubMed: 9808787]
83. Kurokawa M, and Fissore RA (2003). ICSI-generated mouse zygotes exhibit altered calcium oscillations, inositol 1,4,5-trisphosphate receptor-1 down-regulation, and embryo development. Mol. Hum. Reprod 9, 523–533. [PubMed: 12900511]
84. Paudel B, Gervasi MG, Porambo J, Caraballo DA, Tourzani DA, Mager J, Platt MD, Salicioni AM, and Visconti PE (2019). Sperm capacitation is associated with phosphorylation of the testis-specific radial spoke protein Rsph6a†. Biol. Reprod 100, 440–454. [PubMed: 30239614]
85. M. M. (2011). Cutadapt Removes Adapter Sequences from High-Throughput Sequencing Reads.
86. Dobin A, Davis CA, Schlesinger F, Drenkow J, Zaleski C, Jha S, Batut P, Chaisson M, and Gingeras TR (2013). STAR: ultrafast universal RNA-seq aligner. Bioinformatics 29, 15–21. [PubMed: 23104886]
87. Liao Y, Smyth GK, and Shi W (2014). featureCounts: an efficient general purpose program for assigning sequence reads to genomic features. Bioinformatics 30, 923–930. [PubMed: 24227677]
88. Love MI, Huber W, and Anders S (2014). Moderated estimation of fold change and dispersion for RNA-seq data with DESeq2. Genome Biol. 15, 550. [PubMed: 25516281]

Highlights

- Gametes and early embryos express TRPM7 with distinct membrane and nuclear localization
- Preimplantation-stage embryos require TRPM7 function prior to the BL stage
- TRPM7 regulates Mg^{2+} homeostasis and cell division and prevents oxidative stress in embryos
- The channel and kinase domains of TRPM7 contribute to optimizing early embryo development

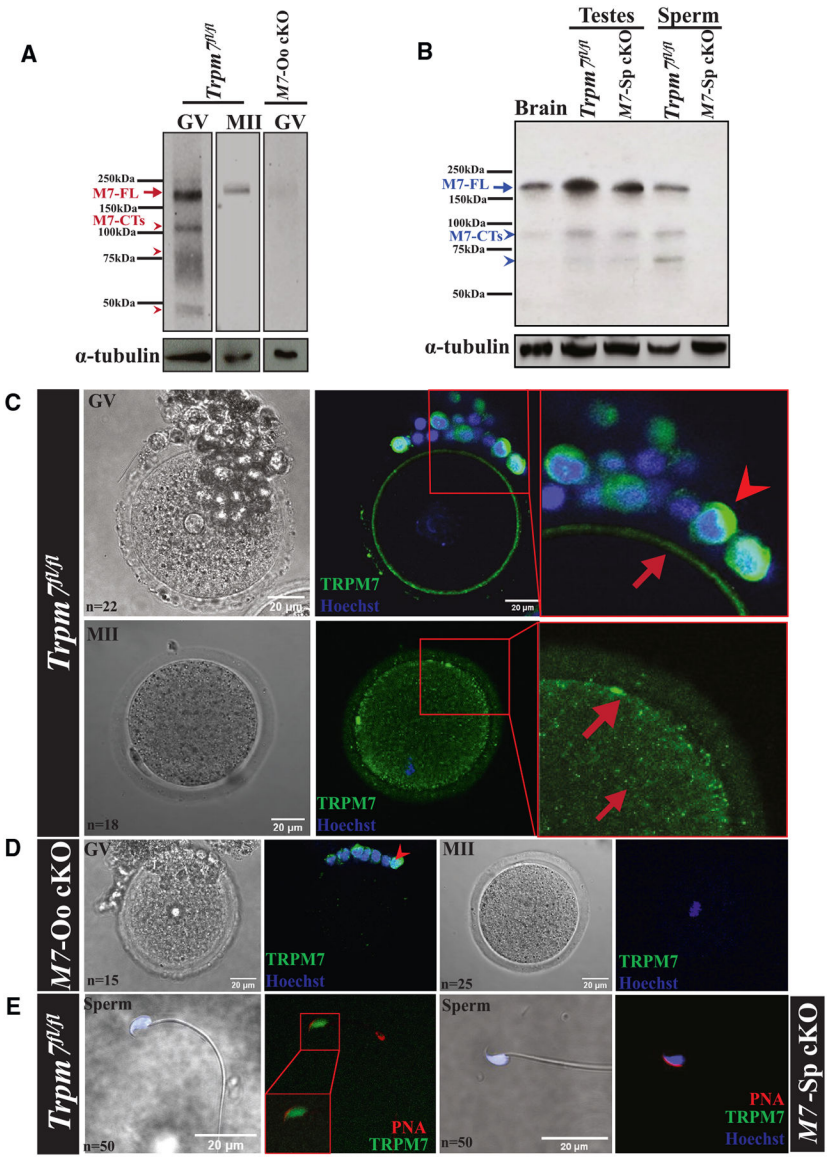

Figure 1. Mouse gametes express TRPM7, and *Trpm7* conditional deletion prevents it

(A) Images of western blots (WBs) of GVs and MIIs denoting expression of full-length TRPM7, M7-FL (red arrow), in *Trpm7*$^{fl/fl}$ oocytes and eggs and lack of it in the adjacent lane in GVs of *Trpm7*-Oo cKO (M7-Oo cKO) females. M7-CTs (red arrowheads) below correspond to C-terminal fragments of the chanzyme. The images below the TRPM7 blots correspond to α-tubulin and were used to normalize TRPM7 expression here and elsewhere. (B) WB of brain tissue, testes, and sperm extracts from *Trpm7*$^{fl/fl}$ and *Trpm7*-Sp cKO (*M7*-Sp cKO) lines showing TRPM7-FL reactivity (blue arrow) and lack of it in the cKO sperm line (rightmost lane). Tissues and sperm also contain M7-CTs (blue arrowheads). (C–E) Bright-field (left column) and immunofluorescence (IF) images of TRPM7 in oocytes and eggs of *Trpm7*$^{fl/fl}$ and *M7*-Oo cKO lines (C and D, respectively) and sperm (E) from *Trpm7*$^{fl/fl}$ and *M7*-Sp cKO lines (two left and right images, respectively). TRPM7 reactivity is in green, DNA in blue, and PNA in red, marking the acrosome. Square red insets in the

upper two rows, center, are enlarged on the right; red arrows denote the TRPM7 position in oocytes/eggs and arrowheads in granulosa cells. (D) and (E) show the absence of TRPM7 reactivity in *M7*-Oo cKO oocytes and eggs and *M7*-Sp cKO sperm, respectively. The white scale bars represent distance in micrometers here and for the rest of the study; n represents the number of observations here and elsewhere.

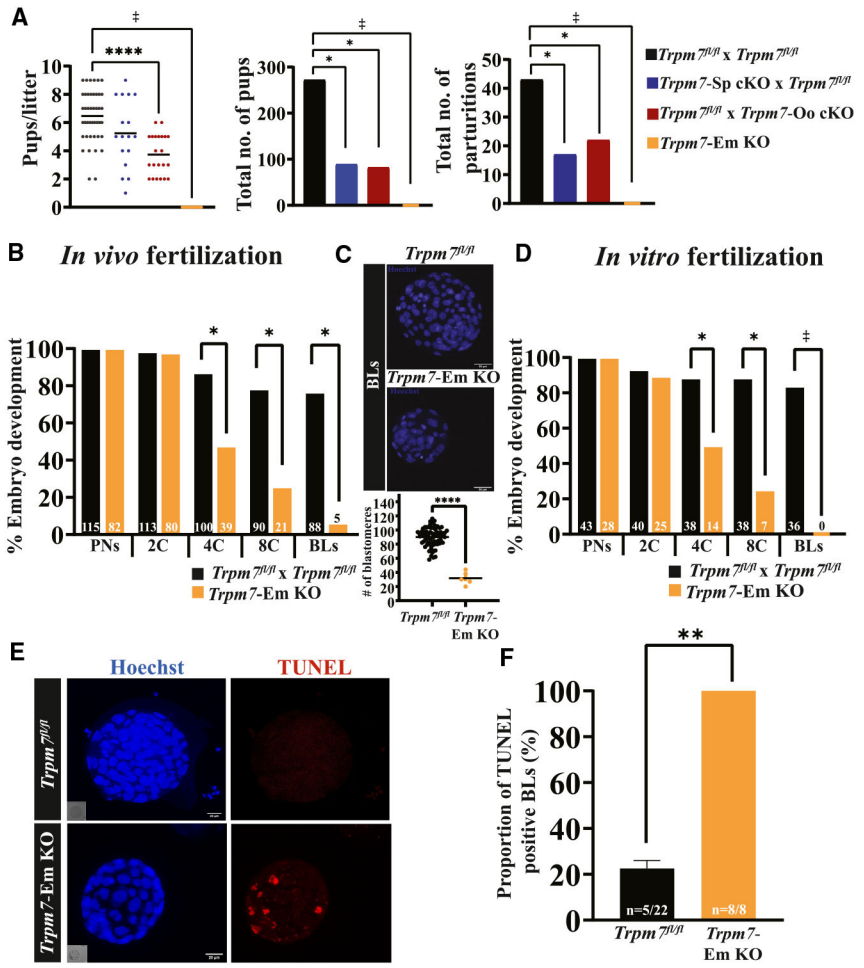

Figure 2. *Trpm7* is a requisite for fertility and preimplantation embryo development

(A) A dot plot and bar graphs depicting the mating outcomes between crosses of *Trpm7*$^{fl/fl}$ mice and breeder lines expressing gamete-specific *Cre*s. Six pairs per group were observed for 6 months, and the numbers of litters, pups, and pups/litter were recorded and statistically compared. Differences between groups were assessed by ANOVA followed by Tukey's *post hoc* test. Asterisks (*) above columns indicate significance between columns/groups here and elsewhere (*$p < 0.05$; ****$p < 0.0001$).

(B–D) Rates of preimplantation development of *Trpm7*$^{fl/fl}$ and *Trpm7*-Em KO zygotes collected after *in vivo* mating (B) or *in vitro* fertilization (D) and cultured *in vitro*. Bar graphs illustrate the embryo stages examined during culture. Data are percentage of embryos reaching each successive stage from PN to BL and the precise numbers noted in the columns. The number of zygotes was the reference (100%). (C) BLs were stained with Hoechst, and nuclei were counted to estimate the number of blastomeres per BL (*$p < 0.05$).

(E) The TUNEL assay was used to determine the presence of apoptotic cells in BLs from *Trpm7*$^{fl/fl}$ and *Trpm7*-Em KO zygotes (red internal fluorescence, right lower image).

(F) Bar graph depicts the proportion of apoptotic BLs in *Trpm7*$^{fl/fl}$ vs. *Trpm7*-Em KO zygotes. Student's t test was applied for comparisons (**$p < 0.01$). The ‡ symbol denotes crosses that did not produce offspring or BLs here and elsewhere in the article.

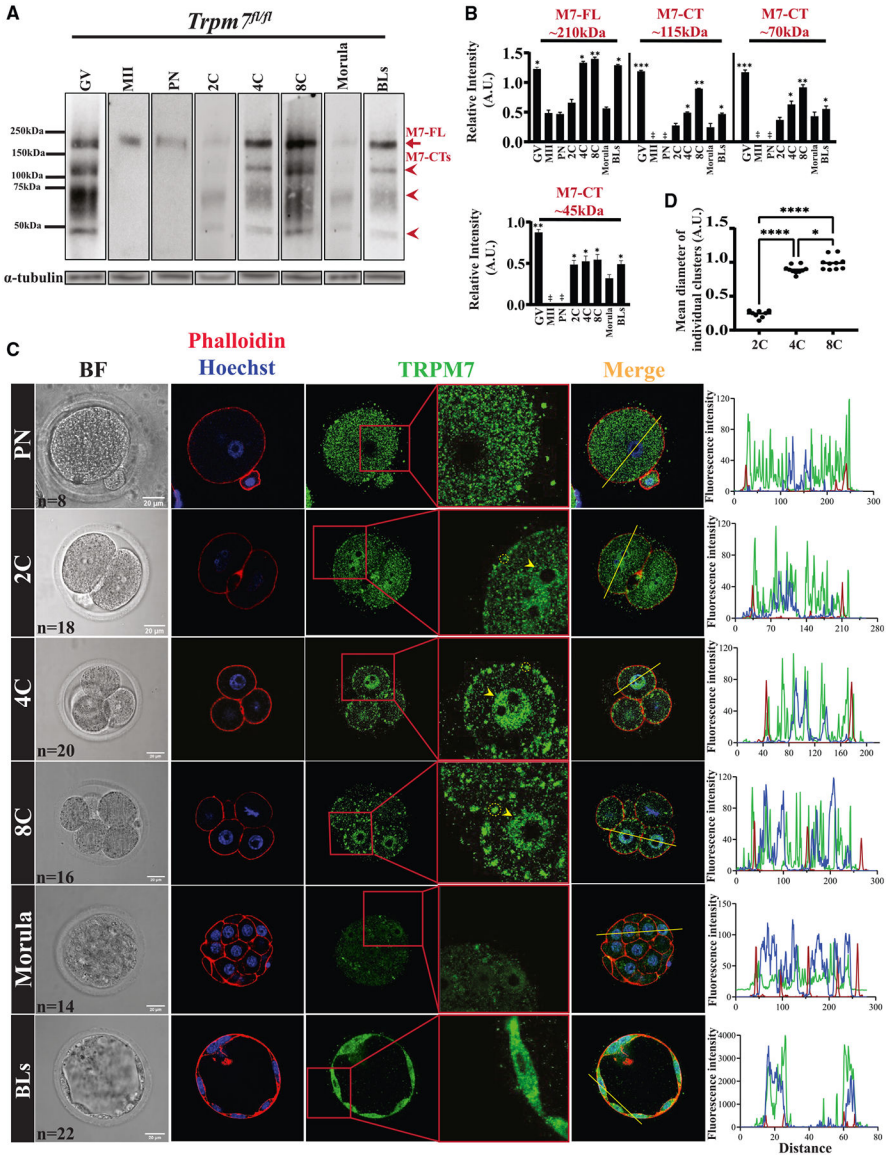

Figure 3. TRPM7 displays stage-specific expression and distinct distributions in preimplantation embryos

(A) WB of TRPM7 reactivity in oocytes, eggs, and preimplantation embryos (n = 50). The red arrow denotes the full-length protein, M7-FL, and the arrowheads denote the three most abundant C-terminal fragments. α-tubulin reactivity is shown below each lane and was used to normalize TRPM7 quantifications.

(B) The relative intensities of M7-FL and M7-CTs between oocytes, eggs, and embryos were quantified from three replicates, statistically compared, and represented by bar graphs. Columns without asterisks are stages with lower and statistically significant expression compared with those with asterisks (*$p < 0.05$, **$p < 0.01$, or ***$p < 0.001$), whereas for the bars with asterisks, a different number of asterisks indicates a difference between groups (*$p < 0.05$ or **$p < 0.01$).

(C) Bright-field (left column) and IF images of PN, 2C, 4C, 8C, morula, and BL stage embryos (remaining columns) displaying actin distribution by phalloidin labeling (red) and

nuclear DNA by Hoechst staining (blue) (second column) and TRPM7 distribution (green; three rightmost columns).A yellow trace in the Merge column denotes the line where the fluorescence was estimated for the three probes. On the right, the line plots display the intensity of the fluorescent signals across the embryos. The number (n) of cells and embryos examined per stage is indicated in the bright-field images, and the white bars represent distance in micrometers.

(D) Comparison of the sizes of the TRPM7 PM clusters observed in the 2C, 4C, and 8C stage embryos (*$p < 0.05$, ****$p < 0.0001$). Comparisons were carried out using ANOVA followed by Tukey's *post hoc* tests.

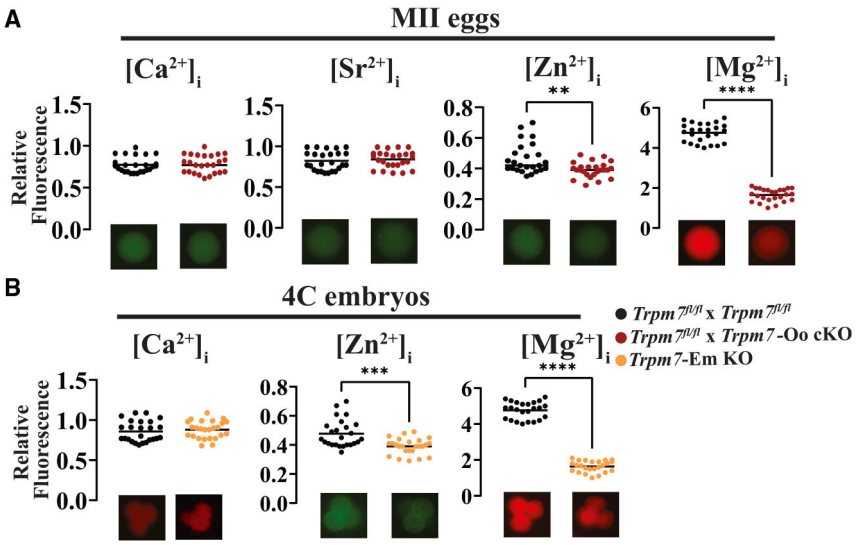

Figure 4. TRPM7 is essential for divalent cation homeostasis in eggs and early embryos

(A) Dot plots displaying normalized intracellular concentrations of the divalent cations Ca^{2+}, Sr^{2+}, Zn^{2+}, and Mg^{2+} (left to right, respectively) in MII eggs from *Trpm7*$^{fl/fl}$ (black) and *Trpm7*-Oo cKO (red) lines (**p < 0.01; ****p < 0.0001).

(B) Dot plots displaying normalized intracellular concentrations of divalent cations in 4C stage embryos; from left to right, Ca^{2+}, Zn^{2+}, and Mg^{2+} from *Trpm7*$^{fl/fl}$ and *Trpm7*-Em KO lines. Representative images are shown below the dot plots to depict differences in fluorescence intensities. Data were compared from at least three experiments using Student's t test (***p < 0.001, ****p < 0.0001).

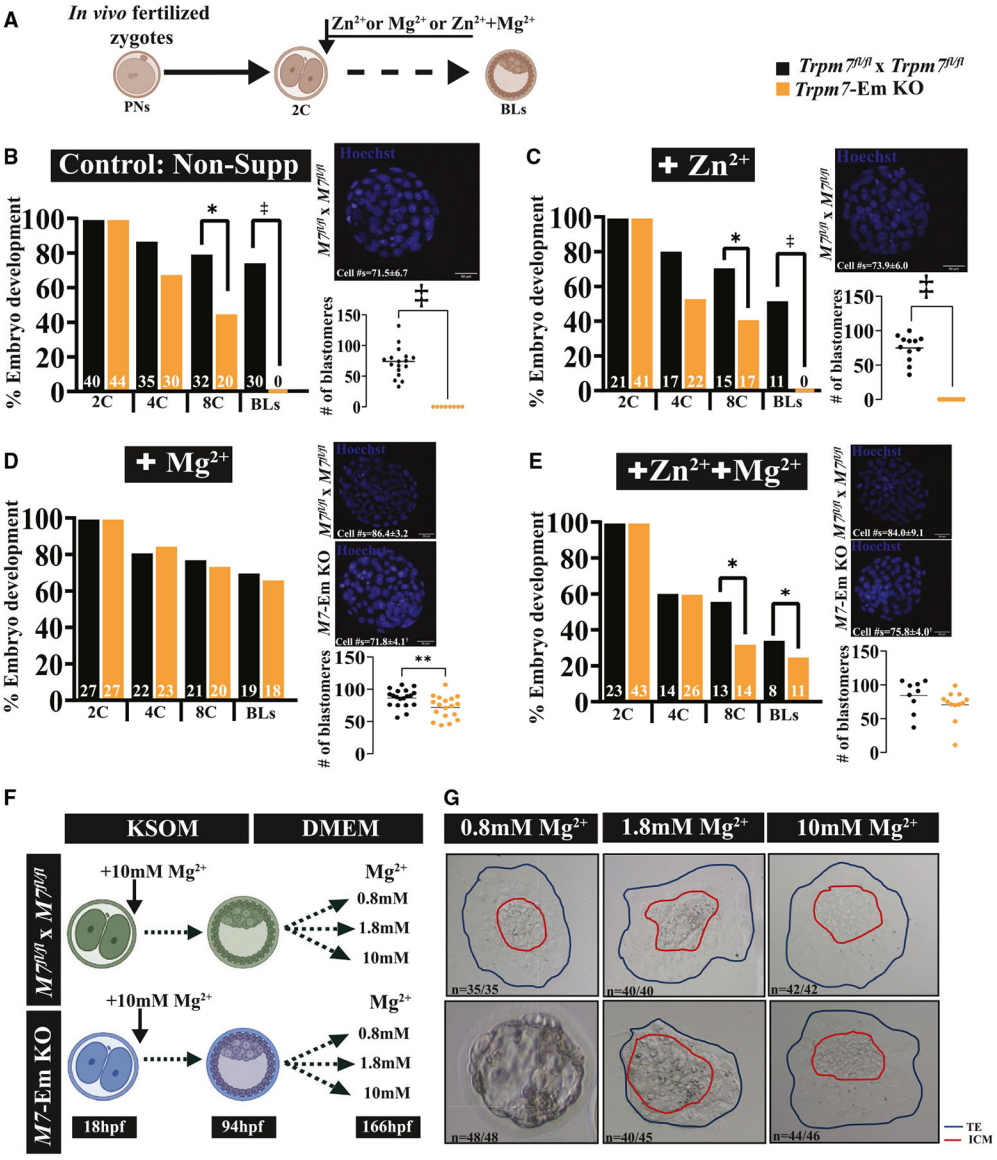

Figure 5. Mg^{2+} supplementation rescues *Trpm7*-Em KO preimplantation embryo development

(A) Schematic of Mg^{2+} supplementation strategy. The extra divalent cations were added at the 2C stage and remained throughout the culture period.

(B–E) Bar graphs depicting rates of *in vitro* preimplantation development of zygotes from *Trpm7*$^{fl/fl}$ and *Trpm7*-Em KO mice in unsupplemented medium (B) or medium supplemented with Zn^{2+} (C), Mg^{2+} (D), or both ions (E). Representative images of BLs stained with Hoechst and BL cell number means in dot charts are displayed for each condition to the right of the graphs.

(F) Schematic of outgrowth assay strategy. *Trpm7*$^{fl/fl}$ and *Trpm7*-Em KO embryos were cultured to the BL stage (94 h post-fertilization [hpf]) in KSOM supplemented with 10 mM Mg^{2+}. After this time, BLs from both groups were transferred to DMEM containing 0.8, 1.8, or 10 mM Mg^{2+} and cultured until 166 hpf.

(G) Representative images of expanded BLs with different concentrations of Mg^{2+} in control and *MZ*-Em KOs. Statistical comparisons were performed using Student's t test ($p > 0.05$ or $*p < 0.05$). The ‡ symbol denotes groups that did not produce BLs and were not statistically compared.

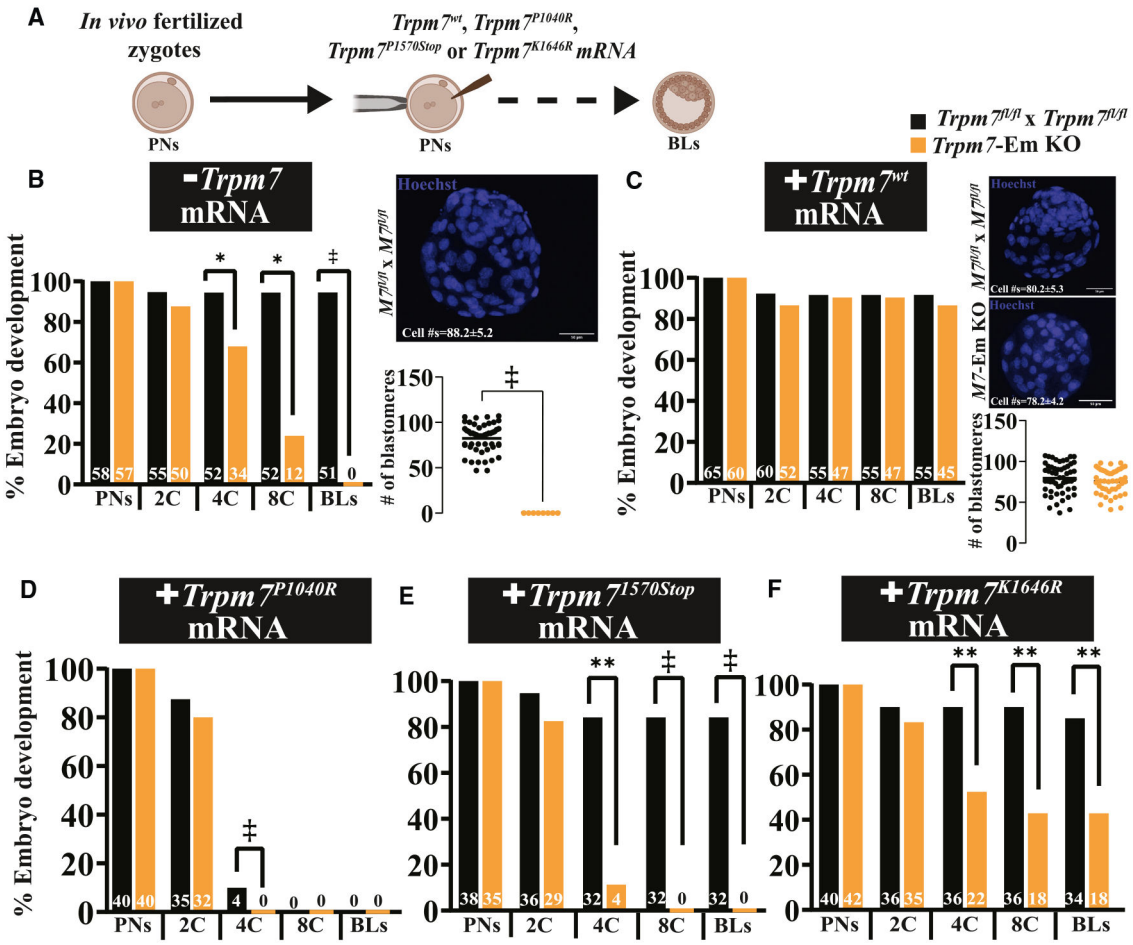

Figure 6. TRPM7^{wt} mRNA rescues *Trpm7*-Em KO embryo development, but mutant versions are not as effective

(A) Schematic of the *Trpm7* mRNA rescue strategy. mRNA injections were always performed into *Trpm7*-Em KO zygotes, after which they were cultured in medium not supplemented with Mg^{2+}.

(B–F) Bar graphs depicting rates of preimplantation embryo development of *Trpm7*$^{fl/fl}$ and *Trpm7*-Em KO uninjected embryos used as controls (*p < 0.05) (B) or embryos injected with *Trpm7*^{wt} (C), *Trpm7*^{P1040R} (D), *Trpm7*^{K1646R} (E), and *Trpm7*^{1570Stop} mRNA (p > 0.05; **p < 0.01). Representative images of BLs stained with Hoechst and cell number quantification are shown to the right of each graph. Statistical comparisons were performed using Student's t test (p > 0.05). The ‡ symbol denotes groups that did not produce BLs and were not statistically compared.

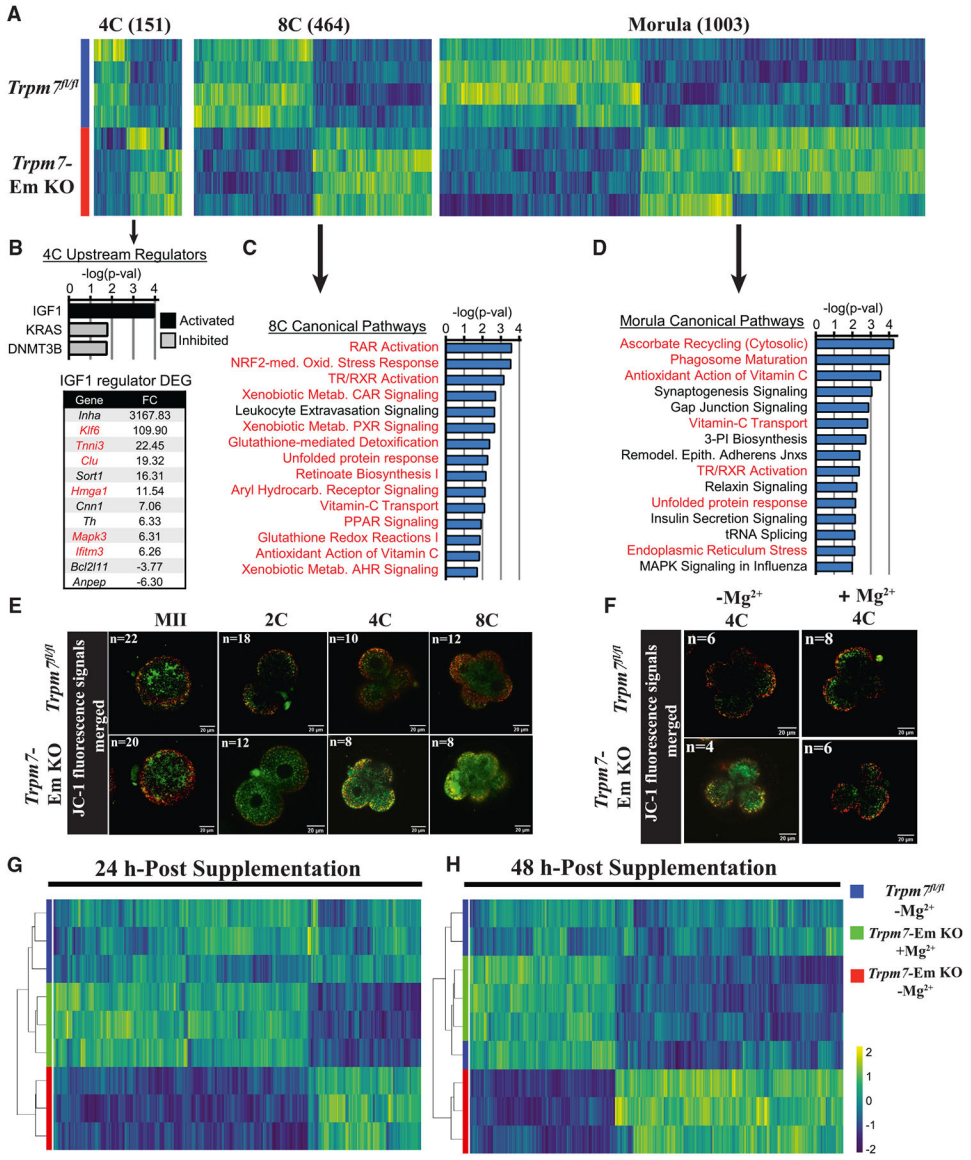

Figure 7. TRPM7 expression prevents oxidative stress in preimplantation embryos by promoting Mg^{2+}influx

(A) Heatmap representation of the comparison of differentially expressed genes (DEGs) identified by RNA-seq in *Trpm7*$^{fl/fl}$ control embryos relative to *Trpm7*-Em KO embryos at the four-cell (4C), 8C, and morula stages. The number of DEGs at each stage is indicated in parentheses above each group.

(B) Ingenuity pathway analysis (IPA) of upstream regulators predicted as activated or inhibited in 4C embryos; $p < 0.05$. DEGs present in the IGF1 upstream regulator dataset and fold change (FC) are shown; red font indicates a role in mitochondrial function, inflammation, or oxidative stress.

(C and D) IPA of canonical pathways in 8C embryos (C) and morulae (D); the 15 most significant pathways relevant to the two embryo stages are shown. The red font indicates oxidative stress-related pathways.

(E and F) Mitochondrial membrane potential as indicated by merged ratio images of JC-1 staining of MII eggs and embryos of the indicated genotypes and cellular stages. Representative images of all embryo stages examined are shown (E). Embryos of both strains were handled as before but supplemented or not with Mg^{2+} at the 2C stage and cultured to the 4C stage (F).

(G and H) Unsupervised hierarchical clustering of DEGs identified by RNA-seq at the indicated time points in *Trpm7*$^{fl/fl}$, *Trpm7*-Em KO, and *Trpm7*-Em KO embryos cultured with and without added Mg^{2+}.

KEY RESOURCES TABLE

REAGENT or RESOURCE	SOURCE	IDENTIFIER
Antibodies		
Goat anti-Mouse IgG (H+L) Cross-Adsorbed Secondary Antibody, HRP	Invitrogen	Cat# G21040; RRID: AB_228307
Goat anti-Mouse IgG (H+L) Highly Cross-Adsorbed Secondary Antibody, Alexa Fluor™ Plus 488	Invitrogen	Cat# A32723; AB_2535764
Hoechst 33342 Solution	Thermo Scientific	62249
Lectin PNA From Arachis hypogaea (peanut), Alexa Fluor™ 568 Conjugate	Invitrogen	L32458
Monoclonal α-tubulin (Mouse monoclonal)	Sigma-Aldrich	T9026
Rhodamine Phalloidin	Invitrogen	R415
TRPM7 (DA5C7)	In-house made	
Biological samples		
Mouse oocytes	Our breeding colonies. This paper	N/A
Mouse preimplantation embryos	This paper-Same.	N/A
Mouse sperm	This paper-Same.	N/A
Chemicals, peptides, and recombinant proteins		
3-Isobutyl-1- methylxanthine (IBMX)	Sigma-Aldrich	I5879
BSA	Sigma-Aldrich	A0281-5G
Ethylenediaminetetraacetic acid sodium dihydrate (EDTA)	LabChem	LC137501
FBS	R&D systems	S11195H
Hyaluronidase from bovine testes	Sigma-Aldrich	H3506
Magnesium sulphate ($MgSO_4.7H_2O$)	Fisher scientific	M63-500
Polyvinylpyrrolidone (PVP)	Sigma-Aldrich	PVP360
Pme1	New England Biolabs	R0560S
Strontium chloride hexahydrate (SrCl2)	Sigma-Aldrich	255521
Zinc Chloride	Fisher scientific	S25635A
Critical commercial assays		
Agencourt AMPure XP kit	Beckman	A63882
High pure RNA isolation kit	Roche	12033674001
Illumina DNA Prep kit	Illumina	20018704
iScript™ cDNA Synthesis Kit	BioRad	1708890
JC-1 Assay	Abcam	Ab113850
Poly(A) Tailing Kit	Invitrogen	AM1350
SMART-Seq v4 Ultra Low Input RNA Kit	Takara	634894
SYBR green master mix	Thermo Fisher	A46012
T7 mMESSAGE mMACHINE Kit	Invitrogen	AM1344
TUNEL Assay Apoptosis Detection Kit	Biotium	CF640R
Deposited data		
Mouse eggs and early embryos RNAseq data	NCBI	GEO: GSE241487
Experimental models: Organisms/strains		

REAGENT or RESOURCE	SOURCE	IDENTIFIER
Mus Musculus Trpm7-floxed	A generous gift from Dr. Carmen P. Williams (NIEHS) (PMID: 30322909)	N/A
Mus Musculus Gdf9-cre	Jackson laboratory	011062
Mus Musculus Hspa2-cre	Jackson laboratory	008870
Mus Musculus BALB/cJ	Jackson laboratory	000651
Oligonucleotides		
Refer to Table S6 for specific primers sequences.		
Recombinant DNA		
pcDNA6-*Trpm7^{wt}-venus*	A generous gift from Dr. Vladimir Chubanov;	N/A
pcDNA6-*Trpm7 ^{P1040R}-venus*	A generous gift from Dr. Vladimir Chubanov; Ludwig-Maximilians-Universitaet Muenchen, Germany.	N/A
pcDNA6-*Trpm7 ^{K1646R}-venus*	This paper-mutations based on manuscripts published by others.	N/A
pcDNA6-*Trpm7^{1570Stop}-venus*	This paper- mutations based on manuscripts published by others.	N/A
pcDNA6-CALR-D1ER-KDEL	Published in previous Fissore lab paper PMID: 24101727 Original D1ER vector was a generous gift from Dr. Roger Y Tsien (PMID: 15585581)	N/A
Software and algorithms		
Prism	GraphPad Software	Version 5.01
ImageJ	NIH	N/A
Other		
BODIPY 500/510	Thermo Scientific	D3823
DMEM	Lonza	12-707F
FluoZin-3 AM	Invitrogen	F24195
Fura-2 AM	Invitrogen	F1221
hCG	Sigma-Aldrich	9002-61-3
Glutamax	Fisher scientific	35-050-061
Mag-Fura-2 AM	Invitrogen	M1292
Pluronic F-127 (20% solution in DMSO) (Pluronic acid)	Invitrogen	P3000MP
PMSG	BioVendor R&D	RP1782725000
Vectashield	Vector Laboratories	H-1500-10